AIMS Mathematics, 10(5): 11514–11555.
DOI: 10.3934/math.2025524
Received: 16 January 2025
Revised: 07 May 2025
Accepted: 08 May 2025
Published: 20 May 2025

https://www.aimspress.com/journal/Math

Research article

Codimension one and codimension two bifurcations analysis of discrete mussel-algae model

Qingkai Xu[1], **Chunrui Zhang**[1] **and Xingjian Wang**[2,*]

[1] College of science, Northeast Forestry University, Harbin 150040, China

[2] College of Computer and Control Engineering, Northeast Forestry University, Harbin 150040, China

* **Correspondence:** Email: jianxingwang@126.com.

Abstract: In this paper, a continuous mussel-algae model was discretized using the explicit Euler method, yielding a discrete mussel-algae interaction model. Within this work, the stability and bifurcations of a discrete mussel-algae model were studied. First, the existence of the unique positive equilibrium point was given. By choosing the time step τ as the bifurcation parameter, we investigated several dynamic behaviors of the model. Using the center manifold theorem and bifurcation theory, the conditions for the existence of codimension-one bifurcations (Flip bifurcation and Neimark-Sacker bifurcation) were derived. Then, by substituting several variables and introducing new parameters, the conditions corresponding to the codimension-two bifurcation (1:2, 1:3, and 1:4 strong resonance) were evaluated. One can identify the existence of different bifurcation forms by essentially calculating the critical non-degeneracy coefficients. The numerical simulations validated the proposed results and illustrated the complicated dynamical behaviors of the mussel algae system. In addition, via numerical simulations, we discovered several pathways through which the system could reach chaos. Specifically, both the Flip bifurcation and the strong resonance bifurcations could eventually guide the system into a chaotic state. These results were distinct from those of the corresponding continuous model, providing a novel perspective for studying the relationship between the population densities of mussels and algae.

Keywords: discrete mussel-algae system; bifurcations; strong resonances; 1:2 resonance; chaos
Mathematics Subject Classification: 34C23, 37N25

1. Introduction

In recent years, with the development of ecological science, the ecosystem has become an important subject in the field of mathematics and biology [1]. Accordingly, researchers have developed diverse ecological models [2, 3] to investigate their dynamic properties, with characteristics such as stability,

bifurcation, and periodic oscillation, attracting significant scientific interest. One of the major challenges in studying population ecosystems lies in the intricate interactions within populations and among species. The use of mathematical models to analyze and simulate these population interactions is a widely adopted and effective research approach.

Mussels possess high nutritional value and serve as significant economic resources in many coastal regions. They primarily feed on algae, phytoplankton, and zooplankton. However, in soft sediment or subtidal mussel beds, the survival and growth of mussels are heavily contingent upon the availability of algal food sources. The quantity of algal intake directly influences the growth dynamics of mussels [4–6]. Moreover, mussels play a crucial role in enhancing ecosystem health [7]. Through their filter-feeding behavior, mussel populations contribute to maintaining water clarity, reducing excessive algae and plankton rich in nitrogen and phosphorus, and mitigating marine eutrophication. Analyzing the interaction between mussels and algae, mathematically modeling the dynamics of these two populations, and investigating their various dynamic behaviors are essential from mathematical and ecological perspectives.

Van De Koppel [8] first proposed a coupled partial differential equation to illustrate the pattern formation process [9, 10] and described the interaction between mussels and algae, considering the corresponding non-diffusive [11–13] form as follows:

$$\begin{cases} \frac{\partial M}{\partial s} = ceMA - d_M \frac{k_M}{k_M + M} M, \\ \frac{\partial A}{\partial s} = (A_{up} - A)\rho - \frac{c}{H} MA, \end{cases} \tag{1.1}$$

where $M = M(s)$ and $A = A(s)$ are the density of mussel and algae at time s, respectively. The consumption coefficient is denoted by c, and e represents the conversion coefficient that relates ingested algae to mussel production. The maximal per capita mussel mortality rate is represented by d_M, and k_M reflects the saturation rate of mussel. A_{up} describes the concentration of algae in the surface layer, whereas ρ represents the exchange rate between the lower and upper water layers. H denotes the height of the lower water layer. All of the above parameters are nonnegative.

The study of model (1.1) has generated significant interest and has led to substantial conclusions. For instance, based on model (1.1), Van De Koppel et al. [8] conducted corresponding experimental studies on the self-organizing patterns of mussels, including field experiments and laboratory tests [14], and studied the influence of the self-organization behavior on the ecosystem of mussel beds [15, 16] from the perspective of ecology. Based on the nonlinear numerical method, Wang et al. [17] analyzed the stability of the linear system of model (1.1), compared the numerical results of the nonlinear system, and focused on the sensitivity of the parameters of model (1.1). Cangelosi et al. [18] investigated the Turing instability and simulated the Turing patterns using nonlinear instability analysis. Song et al. [4, 19] studied the stability of constant normal equilibrium state and Turing-Hopf bifurcations with reaction-diffusion under spatial one-dimensionality and homogeneous Neumann boundary conditions [20], and obtained the dynamic behavior of the system near the bifurcation points by calculating the normal form [21] on the central manifold.

In fact, most of these studies are based on continuous mussel-algae models, and discrete models are rarely discussed. Over the past decades, extensive scholarly investigations have been conducted on diverse discrete mathematical models, yielding substantial theoretical advances. Guckenheimer et al. [22] introduced a calculation method for the normal form of the Flip bifurcation in discrete models. Kuznetsov et al. [23] provided a comprehensive summary of the calculation

methods for the normal forms of several strong resonances. D'Amico et al. [24] developed a method to control the amplitudes and stability of orbits arising from Neimark-Sacker bifurcations in discrete-time systems, utilizing a frequency-domain framework for bifurcation analysis in mappings. Li et al. [25] proposed a class of complex-valued neural network models incorporating both discrete delay and distributed delay, and investigated the Hopf bifurcation problem of the newly proposed complex-valued neural network model.

Generally, discrete models provide better advantages than corresponding continuous models in the study of spatiotemporal dynamics [26, 27]. In the case of the mussel-algae interaction system studied in this paper, statistics for mussels and algae are usually collected and recorded in discrete time, so the discrete mussel-algae model is more suitable and accurate to describe the dynamics of the two species. Besides, computers inherently operate in discrete time, resulting in inevitable inaccuracies when simulating continuous-time systems [28]. Several numerical simulations reveal that the dynamics of discrete-time models are richer than those of corresponding continuous models. For instance, chaotic behaviors are more easily observed in discrete-time dynamics. Consequently, an expanded analysis of the mussel-algae model with discrete time is reasonable.

To simplify parameters, using the following dimensionless transformation [29] to system (1.1), we get

$$t = d_M s,\ x = \frac{M}{k_M},\ y = \frac{A}{A_{up}},\ r = \frac{ecA_{up}}{d_M},\ \alpha = \frac{\rho H}{ck_M},\ \gamma = \frac{d_M H}{ck_M},$$

and then system (1.1) can be reduced as

$$\begin{cases} \frac{dx}{dt} = rxy - \frac{x}{1+x}, \\ \frac{dy}{dt} = \frac{1}{\gamma}[\alpha(1-y) - xy]. \end{cases} \tag{1.2}$$

In this paper, model (1.2) is discretized by the explicit Euler method [30], and then the dynamical properties of the discrete system are discussed. After discretizing model (1.2) by the explicit Euler method, we obtain the following discrete model:

$$\begin{cases} x_{n+1} = x_n + \tau(rx_n y_n - \frac{x_n}{1+x_n}), \\ y_{n+1} = y_n + \frac{\tau}{\gamma}[\alpha(1-y_n) - x_n y_n], \end{cases} \tag{1.3}$$

where $\tau > 0$ refers to the step length of (1.3).

We focus on the nonlinear dynamic behavior and chaos of the two-species mussel-algae system. In a typical ecological scenario, the stable coexistence of mussels and algae is critical for maintaining ecological health. However, parameter variations (such as mussel mortality rates and algal conversion efficiency) induce system destabilization manifested through bifurcation phenomena, including Flip bifurcation, Neimark-Sacker bifurcation, and strong resonance bifurcations. These bifurcation mechanisms establish transition pathways from ordered states to chaos, where long-term unpredictability compromise the effectiveness of ecological monitoring and resource management in mussel-algae systems. We derive stability conditions of the positive equilibrium and bifurcation thresholds to provide mitigation strategies against population outbreaks while maintaining stable mussel-algae symbiosis.

This paper is organized as follows. The existence and stability of fixed points in the discrete model (1.3) are illustrated in Section 2. In Section 3, we discuss some bifurcations of codimension-one, such as the Flip bifurcation and Neimark-Sacker bifurcation occurring in this model. For the

analysis in Section 4, we focus on the codimension-two bifurcations, including 1:2, 1:3, and 1:4 strong resonances [31, 32]. Several numerical simulations are provided to demonstrate the theoretical results. In the conclusion section, we summarize the results of this study and connect the derived results to the ecological dynamics of mussel-algae populations.

2. Stability of the positive fixed points

By simple calculation, the unique positive equilibrium of system (1.3) is

$$E^*(x^*, y^*) = (\frac{\alpha(r-1)}{1-\alpha r}, \frac{1-\alpha r}{r(1-\alpha)}),$$

and the positive point exists if one of the conditions hold:

$$0 < \frac{1}{\alpha} < r < 1, \ or \ \ 0 < \alpha < \frac{1}{r} < 1.$$

Let

$$\Omega = \frac{1-\alpha}{1-\alpha r},$$

then

$$E^*(x^*, y^*) = (\Omega - 1, \frac{1}{r\Omega}).$$

The Jacobian matrix of the model (1.3) evaluated at the fixed point $E^*(x^*, y^*)$ can be expressed as

$$J(E^*) = \begin{pmatrix} 1 + \frac{\tau(\Omega-1)}{\Omega^2} & \tau r(\Omega - 1) \\ -\frac{\tau}{r\gamma\Omega} & 1 - \frac{\tau\alpha r\Omega}{\gamma} \end{pmatrix}. \tag{2.1}$$

The characteristic equation of $J(E^*)$ is

$$F(\lambda) = \lambda^2 + (G\tau - 2)\lambda + 1 - G\tau + H\tau^2,$$

where

$$G = \frac{\alpha r\Omega}{\gamma} - \frac{\Omega - 1}{\Omega^2}, \ H = \frac{\alpha(r-1)}{\gamma\Omega},$$

and it can be obtained that

$$F(1) = H\tau^2.$$

If $F(1) < 0$, that is $H < 0$, which means that at least one of the eigenvalues has a modulus larger than 1, and as a result, the fixed point is necessarily unstable. In the following discussion, we analyze the stability of equilibria satisfying condition $H \geq 0$.

By simple calculations, we can obtain the following Lemma 2.1.

Lemma 2.1. *The stability of the unique positive equilibrium $E^*(x^*, y^*)$ has the following situations:*

(1) It is locally asymptotically stable if one of the following conditions holds:

i. $H > 0, G^2 > 4H,$ *and* $0 < \tau < \frac{G - \sqrt{G^2 - 4H}}{H}$;

ii. $H > 0, G^2 \leq 4H,$ *and* $0 < \tau < \frac{G}{H}$.

(2) It is unstable if one of the following conditions holds:

i. $H > 0, G < 0$;

ii. $H > 0, G^2 \leq 4H$ *and* $\tau > \frac{G}{H}$;

iii. $H > 0, G^2 > 4H$ *and* $\frac{G-\sqrt{G^2-4H}}{H} < \tau < \frac{G+\sqrt{G^2-4H}}{H}$, *or* $\tau > \frac{G+\sqrt{G^2-4H}}{H}$.

(3) A codimension-one bifurcation may occur if any of the following conditions are satisfied:

i. Flip bifurcation occurs if $H > 0$, $G^2 > 4H$ *and* $\tau = \frac{G-\sqrt{G^2-4H}}{H}$, $\tau \neq \frac{2}{G}, \frac{4}{G}$;

ii. Neimark-Sacker bifurcation occurs if $H > 0$, $G^2 < 4H$ *and* $\tau = \frac{G}{H}$.

(4) A codimension-two bifurcation may occur if any of the following conditions are satisfied:

i. 1:2 strong resonance occurs if $H = \frac{G^2}{4}, G \neq 0$ *and* $\tau = \frac{4}{G}$;

ii. 1:3 strong resonance occurs if $H = \frac{G^2}{3}, G \neq 0$ *and* $\tau = \frac{3}{G}$;

iii. 1:4 strong resonance occurs if $H = \frac{G^2}{2}, G \neq 0$ *and* $\tau = \frac{2}{G}$.

Proof. To facilitate discussion, we assume that two roots of $F(\lambda)$ are

$$\lambda_1 = 1 - \frac{\tau(G + \sqrt{G^2 - 4H})}{2}, \ \lambda_2 = 1 - \frac{\tau(G - \sqrt{G^2 - 4H})}{2}.$$

(1) If $G^2 \leq 4H$, then λ_1 and λ_2 are a pair of conjunctive complex roots and satisfy $\lambda_1\lambda_2 = \left|\lambda_{1,2}\right|^2 = 1 - G\tau + H\tau^2$, so we need only $\left|\lambda_{1,2}\right|^2 < 1$, that is $0 < \tau < \frac{G}{H}$. If $G^2 > 4H$, then $G + \sqrt{G^2 - 4H} > G - \sqrt{G^2 - 4H} > 0$, so we need only $|\lambda_1| < 1$, that is $0 < \tau < \frac{G-\sqrt{G^2-4H}}{H}$.

(2) By simple calculation, we can obtain the conditions *i* and *ii*. If $G^2 > 4H$, then $\lambda_1 < \lambda_2$. The fixed point is unstable when $|\lambda_1| > 1$, or $|\lambda_2| > 1$, which is equivalent to $\lambda_2 < -1$, or, $\lambda_1 < -1$ and $-1 < \lambda_2 < 1$, then we can acquire the condition *iii*.

(3) For the condition *i*, Flip bifurcation occurs if $\lambda_1 = -1$, $|\lambda_2| < 1$, so the condition $G^2 > 4H$ must be satisfied, and according to the expression $\lambda_1 = 1 - \frac{\tau(G+\sqrt{G^2-4H})}{2} = -1$, we have $\tau = \frac{G-\sqrt{G^2-4H}}{H}$; For the condition *ii*, Neimark-Sacker bifurcation occurs when $\lambda_{1,2}$ are a pair of conjugate complex roots with $\left|\lambda_{1,2}\right| = 1$, which yields $\tau = \frac{G}{H}$. In addition, the condition $G^2 < 4H$ must hold to ensure that the characteristic roots are complex conjugates.

(4) 1:2 resonance bifurcation occurs around $E^*(x^*, y^*)$ if $\lambda_{1,2} = -1$, that is $H = \frac{G^2}{4}, G \neq 0, \tau = \frac{4}{G}$. If $\lambda_{1,2} = \frac{-1\pm\sqrt{3}i}{2}$, we have $H = \frac{G^2}{3}, G \neq 0, \tau = \frac{3}{G}$, then 1:3 resonance behavior at $E^*(x^*, y^*)$ will be observed. If $\lambda_{1,2} = \pm i$, we can obtain $H = \frac{G^2}{2}$, $G \neq 0$, $\tau = \frac{2}{G}$, which means that model (1.3) exhibits 1:4 strong resonance around $E^*(x^*, y^*)$.

□

3. Codimension-one bifurcation analysis

3.1. Flip bifurcation

First, we point out how model (1.3) undergoes Flip bifurcation around its unique positive equilibrium $E^*(x^*, y^*) = (\Omega - 1, \frac{1}{r\Omega})$ when τ is selected as the bifurcation parameter. The necessary condition for the occurrence of a Flip bifurcation is determined by the following parameter space:

$$U = \left\{(\alpha, r, \gamma, \tau) \in \mathbb{R}_+^4 : \tau = \tau^* = \frac{G - \sqrt{G^2 - 4H}}{H}, G^2 > 4H, H > 0, \tau^* \neq \frac{2}{G}, \frac{4}{G}\right\}.$$

3.1.1. Existence condition of Flip bifurcation at $E^*(x^*, y^*)$

The Jacobian matrix $J(x, y)$ evaluated at the unique positive equilibrium $E^*(x^*, y^*)$ is the same as that of (2.1). Let $X_n = x_n - x^*, Y_n = y_n - y^*$, which transforms the positive equilibrium $E^*(x^*, y^*)$ to point $(0, 0)$ and model (1.3) to

$$\begin{cases} X_{n+1} = X_n + \tau[r(X_n + x^*)(Y_n + y^*) - \frac{X_n + x^*}{1 + X_n + x^*}], \\ Y_{n+1} = Y_n + \frac{\tau}{\gamma}[\alpha(1 - Y_n - y^*) - (X_n + x^*)(Y_n + y^*)]. \end{cases} \tag{3.1}$$

Notice that $x^* = \Omega - 1$, $y^* = \frac{1}{r\Omega}$, and we use Taylor expansion at the origin yields the following expression:

$$\begin{pmatrix} X_{n+1} \\ Y_{n+1} \end{pmatrix} = \begin{pmatrix} 1 + \frac{\tau(\Omega-1)}{\Omega^2} & \tau r(\Omega - 1) \\ -\frac{\tau}{r\gamma\Omega} & 1 - \frac{\tau\alpha r\Omega}{\gamma} \end{pmatrix} \begin{pmatrix} X_n \\ Y_n \end{pmatrix} + \tau \begin{pmatrix} \varphi(X_n, Y_n) \\ \psi(X_n, Y_n) \end{pmatrix}, \tag{3.2}$$

where

$$\varphi(X_n, Y_n) = a_{13}{X^2}_n + a_{14}X_nY_n + a_{15}{Y_n}^2 + a_{16}{X_n}^3 + a_{17}{X_n}^2Y_n + a_{18}X_n{Y_n}^2 + a_{19}{Y_n}^3 + O((|X_n| + |Y_n|)^4),$$
$$\psi(X_n, Y_n) = a_{23}{X^2}_n + a_{24}X_nY_n + a_{25}{Y_n}^2 + a_{26}{X_n}^3 + a_{27}{X_n}^2Y_n + a_{28}X_n{Y_n}^2 + a_{29}{Y_n}^3 + O((|X_n| + |Y_n|)^4),$$
$$a_{13} = \tfrac{1}{\Omega^3},\ a_{14} = r,\ a_{15} = a_{16} = a_{17} = a_{18} = 0,\ a_{19} = -\tfrac{1}{\Omega^4},\ a_{23} = 0,\ a_{24} = -\tfrac{1}{\gamma},$$
$$a_{25} = a_{26} = a_{27} = a_{28} = a_{29} = 0.$$

We impose a small perturbation δ on the parameter τ, i.e., $\tau = \tau^* + \delta, |\delta| \ll 1$, and the system (3.2) becomes

$$\begin{pmatrix} X_{n+1} \\ Y_{n+1} \end{pmatrix} = \begin{pmatrix} 1 + \frac{(\tau^*+\delta)(\Omega-1)}{\Omega^2} & (\tau^* + \delta)r(\Omega - 1) \\ -\frac{(\tau^*+\delta)}{r\gamma\Omega} & 1 - \frac{(\tau^*+\delta)\alpha r\Omega}{\gamma} \end{pmatrix} \begin{pmatrix} X_n \\ Y_n \end{pmatrix} + (\tau^* + \delta) \begin{pmatrix} \varphi(X_n, Y_n) \\ \psi(X_n, Y_n) \end{pmatrix}. \tag{3.3}$$

The characteristic polynomial of the Jacobian matrix of (3.3) is expressed by

$$g(\lambda) = \lambda^2 - p\lambda + q,$$

where

$$p = 2 + (\tau^* + \delta)(\tfrac{\Omega-1}{\Omega^2} - \tfrac{\alpha r\Omega}{\gamma}),\quad q = \tfrac{\Omega r[-1+\Omega](\delta+\tau^*)^2 - r\left(\Omega^2 + (-1+\Omega)(\tau^*+\delta)\right)(-\gamma+\Omega r\alpha(\tau^*+\delta))}{\Omega^2 r\gamma}.$$

The transversal condition with respect to $E^*(x^*, y^*)$ is

$$\left.\frac{dg(\lambda)}{d\delta}\right|_{\lambda=-1,\delta=0} = \frac{-2r\left(\Omega^3 r\alpha + \gamma + \Omega^2 r\alpha\tau - \Omega\left(\gamma + r\alpha\tau\right)\right) + 2\Omega\tau r(-1 + \Omega)}{\Omega^2 r\gamma}.$$

If $\left.\frac{dg(\lambda)}{d\delta}\right|_{\lambda=-1,\delta=0} \neq 0$, then Flip bifurcation will appear around $E^*(x^*, y^*)$.

3.1.2. The direction of Flip bifurcation at $E^*(x^*, y^*)$

To facilitate discussion, define

$$A = \begin{pmatrix} 1 + \frac{\tau^*(\Omega-1)}{\Omega^2} & \tau^* r(\Omega-1) \\ -\frac{\tau^*}{r\gamma\Omega} & 1 - \frac{\tau^*\alpha r\Omega}{\gamma} \end{pmatrix}.$$

Next, we intend to simplify the model (3.3) through variable substitution. According to the eigenvalue distribution of the Flip bifurcation, at this time, the system has one eigenvalue which is equal to -1, denoted as λ_{11}. The other eigenvalue has a modulus less than 1, which is denoted as λ_{12}. We calculate the eigenvectors corresponding to the two eigenvalues, respectively. The eigenvector corresponding to $\lambda_{11} = -1$ is $\xi_1 = \left(\tau^* r(\Omega-1), -2 - \frac{\tau^*(\Omega-1)}{\Omega^2}\right)^T$, and the eigenvector corresponding to λ_{12} is $\xi_2 = \left(\tau^* r(\Omega-1), \lambda_{12} - 1 - \frac{\tau^*(\Omega-1)}{\Omega^2}\right)^T$. Then, we have the invertible matrix

$$T = \begin{pmatrix} \xi_1 & \xi_2 \end{pmatrix} = \begin{pmatrix} \tau^* r(\Omega-1) & \tau^* r(\Omega-1) \\ -2 - \frac{\tau^*(\Omega-1)}{\Omega^2} & \lambda_{12} - 1 - \frac{\tau^*(\Omega-1)}{\Omega^2} \end{pmatrix},$$

and its inverse matrix

$$T^{-1} = \begin{pmatrix} \frac{-1+\lambda_{12} - \frac{\tau^*(-1+\Omega)}{\Omega^2}}{\tau^* r(-1+\Omega)(1+\lambda_{12})} & -\frac{1}{1+\lambda_{12}} \\ \frac{2+\frac{\tau^*(-1+\Omega)}{\Omega^2}}{\tau^* r(-1+\Omega)(1+\lambda_{12})} & -\frac{1}{1+\lambda_{12}} \end{pmatrix}.$$

We use the transformation

$$\begin{pmatrix} X_{n+1} \\ Y_{n+1} \end{pmatrix} = T \begin{pmatrix} u_{n+1} \\ v_{n+1} \end{pmatrix},$$

and then system (3.3) can be changed into

$$\begin{pmatrix} u_{n+1} \\ v_{n+1} \end{pmatrix} = \begin{pmatrix} -1 & 0 \\ 0 & \lambda_{12} \end{pmatrix} \begin{pmatrix} u_n \\ v_n \end{pmatrix} + \begin{pmatrix} f_1(X_n, Y_n, \delta) \\ g_1(X_n, Y_n, \delta) \end{pmatrix}, \tag{3.4}$$

where

$$\begin{aligned} f_1(X_n, Y_n, \delta) =& B_{11}X\delta + B_{12}Y\delta + C_{11}X^2 + C_{12}XY + C_{13}Y^2 + C_{14}X^3 + C_{15}X^2Y + C_{16}XY^2 + C_{17}Y^3 \\ &+ D_{11}X^2\delta + D_{12}XY\delta + D_{13}Y^2\delta + O((|X| + |Y| + |\delta|)^4), \\ g_1(X_n, Y_n, \delta) =& B_{21}X\delta + B_{22}Y\delta + C_{21}X^2 + C_{22}XY + C_{23}Y^2 + C_{24}X^3 + C_{25}X^2Y + C_{26}XY^2 + C_{27}Y^3 \\ &+ D_{21}X^2\delta + D_{22}XY\delta + D_{23}Y^2\delta + O((|X| + |Y| + |\delta|)^4), \end{aligned}$$

here, the specific expressions for B_{ij}, C_{ij}, and D_{ij} are given in Appendix A.

To facilitate calculation, we set

$$T = \begin{pmatrix} \tau^* r(\Omega-1) & \tau^* r(\Omega-1) \\ -2 - \frac{\tau^*(\Omega-1)}{\Omega^2} & \lambda_{12} - 1 - \frac{\tau^*(\Omega-1)}{\Omega^2} \end{pmatrix} = \begin{pmatrix} T_{11} & T_{12} \\ T_{21} & T_{22} \end{pmatrix}.$$

Using transformation $\begin{pmatrix} X_n \\ Y_n \end{pmatrix} = T \begin{pmatrix} u_n \\ v_n \end{pmatrix}$, system (3.4) becomes

$$\begin{pmatrix} u_{n+1} \\ v_{n+1} \end{pmatrix} = \begin{pmatrix} -1 & 0 \\ 0 & \lambda_{12} \end{pmatrix} \begin{pmatrix} u_n \\ v_n \end{pmatrix} + \begin{pmatrix} f_2(u_n, v_n, \delta) \\ g_2(u_n, v_n, \delta) \end{pmatrix}, \tag{3.5}$$

where

$$\begin{aligned} f_2(u_n, v_n, \delta) =& m_{11}u_n\delta + m_{12}v_n\delta + m_{13}u_n^2 + m_{14}u_nv_n + m_{15}v_n^2 + m_{16}u_n^3 + m_{17}u_n^2v_n + m_{18}u_nv_n^2 + m_{19}v_n^3 \\ &+ q_{11}u_n^2\delta + q_{12}v_n^2\delta + q_{13}u_nv_n\delta + O((|u_n| + |v_n| + |\delta|)^4), \\ g_2(u_n, v_n, \delta) =& m_{21}u_n\delta + m_{22}v_n\delta + m_{23}u_n^2 + m_{24}u_nv_n + m_{25}v_n^2 + m_{26}u_n^3 + m_{27}u_n^2v_n + m_{28}u_nv_n^2 + m_{29}v_n^3 \\ &+ q_{21}u_n^2\delta + q_{22}v_n^2\delta + q_{23}u_nv_n\delta + O((|u_n| + |v_n| + |\delta|)^4). \end{aligned}$$

Here, the specific expressions for m_{ij} and q_{ij} are given in Appendix B.

The central manifold theorem claims that there exists a three-dimensional central manifold $W^c(0)$:

$$W^c{}_{loc}(0) = \left\{(u_n, v_n, \delta) \in \mathbb{R}^3 : v_n = h(u_n, \delta) = j_1{u_n}^2 + j_2u_n\delta + j_3\delta^2 + O((|u_n| + |\delta|)^3)\right\},$$

and must satisfy the following quasilinear partial difference equation:

$$N(h(x)) = h(-u_n + f_2(u_n, h(u_n, \delta), \delta), \delta) - \lambda_{12}h(u_n, \delta) - g_2(u_n, h(u_n, \delta), \delta) = 0,$$

where u_n and δ are sufficiently small.

It can be obtained by balancing powers of coefficients for each component:

$$j_1 = \frac{m_{23}}{1-\lambda_{12}} = \frac{C_{21}{T_{11}}^2 + C_{22}T_{11}T_{21} + C_{23}{T_{21}}^2}{1-\lambda_{12}},\ j_2 = -\frac{m_{21}}{1+\lambda_{12}} = -\frac{B_{21}T_{11} + B_{22}T_{21}}{1+\lambda_{12}},\ j_3 = 0.$$

Hence, the system restricted to the central manifold $W^c{}_{loc}(0)$ is expressed by

$$\Theta : u_n \mapsto -u_n + \vartheta_1{u_n}^2 + \vartheta_2u_n\delta + \vartheta_3{u_n}^2\delta + \vartheta_4u_n\delta^2 + \vartheta_5{u_n}^3 + O((|u_n| + |\delta|)^4),$$

where

$$\vartheta_1 = m_{13}, \vartheta_2 = m_{11}, \vartheta_3 = m_{12}j_1 + m_{14}j_2, \vartheta_4 = m_{12}j_2, \vartheta_5 = m_{16} + m_{14}j_1.$$

Then, we need to calculate the following two coefficients at $(u, v, \delta) = (0, 0, 0)$:

$$\begin{aligned} \alpha_1 &= \left(\frac{\partial^2 F}{\partial u_n \partial \delta} + \frac{1}{2}\frac{\partial F}{\partial \delta}\frac{\partial^2 F}{\partial {u_n}^2}\right)\Big|_{(0,0)} = \vartheta_2, \\ \alpha_2 &= \left(\frac{1}{6}\frac{\partial^3 F}{\partial {u_n}^3} + \left(\frac{1}{2}\frac{\partial^2 F}{\partial {u_n}^2}\right)^2\right)\Big|_{(0,0)} = \vartheta_5 + {\vartheta_1}^2. \end{aligned}$$

The following theorem can be obtained:

Theorem 3.1. *If $\alpha_1 \neq 0$, $\alpha_2 \neq 0$ and the condition $(A_3)(i)$ of Lemma 2.1 hold, then the model (1.3) will undergo a Flip bifurcation at the positive equilibrium point $E^*(x^*, y^*)$ when parameter τ fluctuates within a small region of U. Furthermore, when $\alpha_2 > 0$ (resp., $\alpha_2 < 0$), then the Flip bifurcation is supercritical (resp., subcritical) and model (1.3) bifurcates into a periodic two stable(resp., unstable) orbit from the positive equilibrium $E^*(x^*, y^*)$.*

Remark 3.1. *When parameter τ exceeds a critical threshold, the system transitions from a stable equilibrium state (where the population sizes of both algae and mussels remain constant) to a period-2 oscillatory state (alternating between high algae-low mussel and low algae-high mussel phases). The occurrence of cycle doubling indicates that the populations of mussels and algae experience greater fluctuations and longer periodic cycles, which may increase the risk of overexploitation of habitat resources or localized extinction.*

3.1.3. Numerical simulation of Flip bifurcation

We choose τ as the bifurcation parameter in the parameter space U to study the dynamical properties of system (1.3) at $E^*(x^*, y^*)$. We choose the following parameters to discuss.

The unique positive equilibrium point $(x_0, y_0) \approx (1.134146341, 0.209183)$ of the model (1.3) can be obtained by giving the parameters

$$\tau = 1.974187040081111, \alpha = 0.3, r = 2.24, \gamma = 1.$$

The two eigenvalues are $\lambda_{11} = -0.9999999993225626$, $\lambda_{12} = 0.6603236257522207$, and by choosing the initial value of $(\tilde{x}_0, \tilde{y}_0) = (1.134, 0.209)$, we can calculate the coefficients α_1, α_2, and we have

$$\alpha_1|_{(\tilde{x}_0,\tilde{y}_0)} = -0.004319555 \neq 0, \alpha_2|_{(\tilde{x}_0,\tilde{y}_0)} = 833.004325931787 > 0,$$

so according to Theorem 3.1, system (1.3) undergoes a supercritical Flip bifurcation around $(\tilde{x}_0, \tilde{y}_0)$ and bifurcates to a two-periodic stable orbit. The result can be obtained by numerical simulation as Figures 1 and 2.

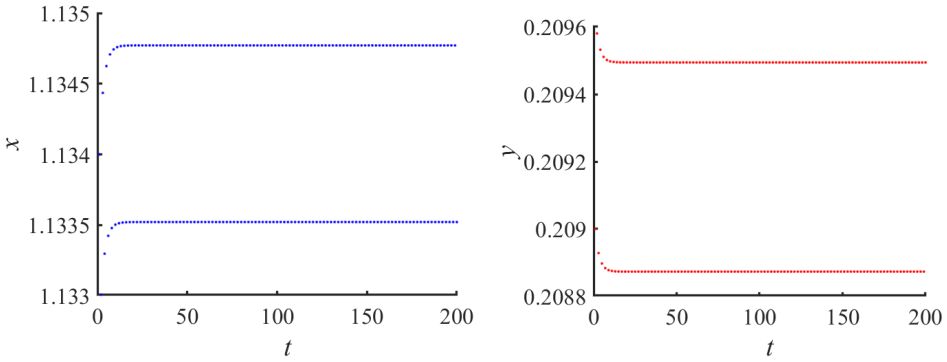

(a) (b)

Figure 1. Flip bifurcation appears around the positive point $(\tilde{x}_0, \tilde{y}_0) = (1.134, 0.209)$. The stable period-two orbit for the variables x and y are shown in (a) and (b), respectively.

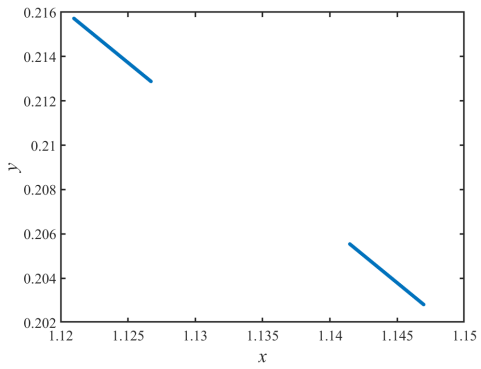

Figure 2. Phase diagrams at point $(\tilde{x}_0, \tilde{y}_0) = (1.134, 0.209)$. There exists a 2-periodic stable orbit around the point $(x_0, y_0) \approx (1.134146341, 0.209183)$.

The relevant perturbation $\delta \in (0, 0.7)$ -bifurcation diagram with step length parameter τ is displayed in Figure 3. Moreover, when we take a particular parameter $\delta = 0.66$, that is, $\tau = 2.634187040081111$, the corresponding phase diagram of the model (1.3) is shown in Figure 4(c), which shows that the chaotic behaviors occur with the increase of the perturbation δ. Figure 4(a) and (b) are the variations of x and y with the time t, respectively.

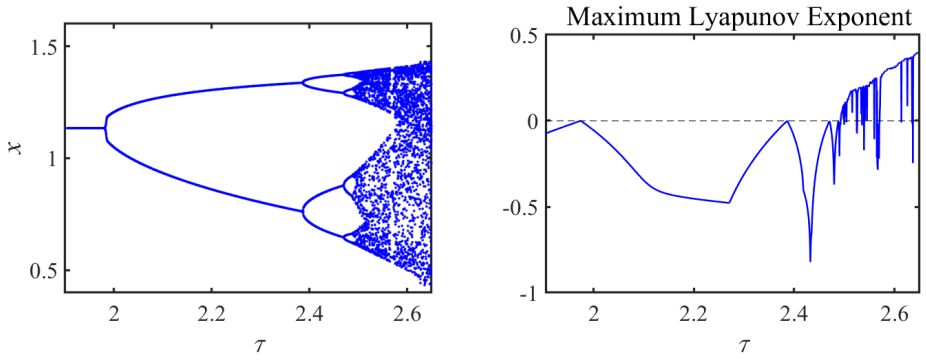

Figure 3. $\delta \in (0, 0.7)$-bifurcation diagram and the maximum Lyapunov exponent with step length τ at the fixed point $(1.134, 0.209)$.

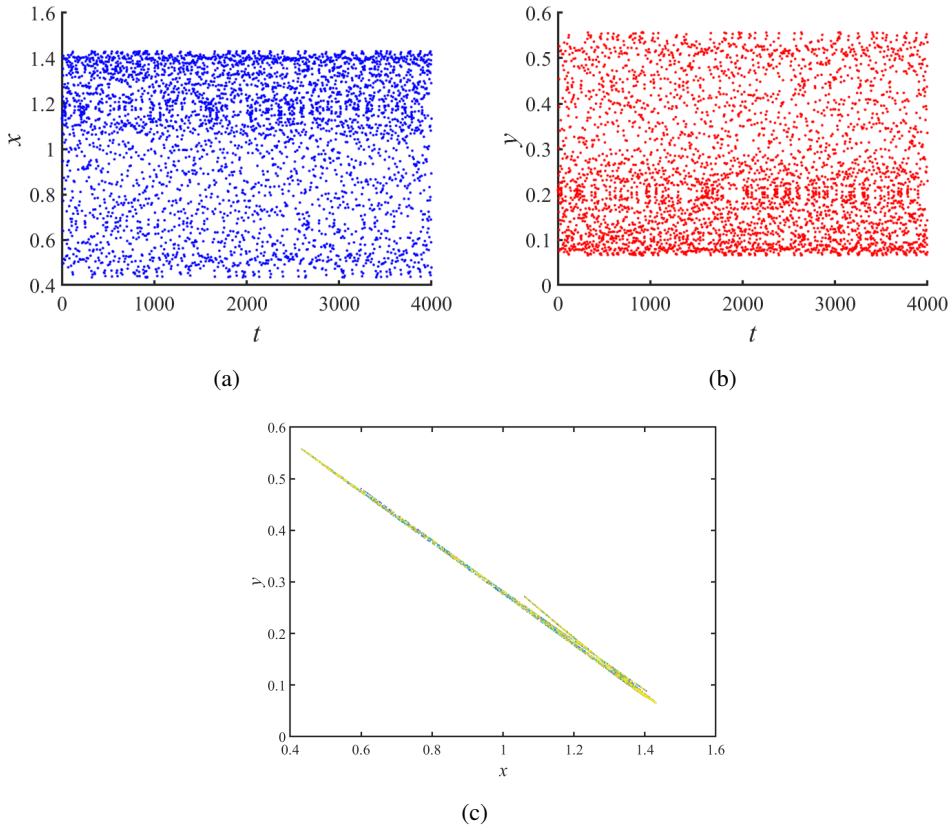

Figure 4. (a) and (b) are the variations of x and y with the time t, respectively. (c) The phase diagram of the system (1.3) at the fixed point $(1.134, 0.209)$. This indicates that chaos occurs in narrow banded regions when the perturbation increases into $\delta = 0.66$.

In biology, Figure 3 shows the phenomenon of mussel population from a stable state through Flip bifurcation and gradually transition to cycle 2, 4, 8, and so on, and finally to chaos. Chaos means that mussel population changes have become unpredictable, and mussel population outbreaks upset the balance of the ecosystem.

3.2. Neimark-Sacker bifurcation

Next, we study the Neimark-Sacker bifurcation of $E^*(x^*, y^*)$ of model (1.3) and select τ as the bifurcation parameter. The following parameter space determines the essential condition for Neimark-Sacker bifurcation to occur:

$$N.S = \left\{(\alpha, r, \gamma, \tau) \in \mathbb{R}_+^4 : \tau = \tau_1{}^* = \frac{G}{H}, G^2 < 4H, H > 0\right\}.$$

3.2.1. Existence condition of Neimark-Sacker bifurcation at $E^*(x^*, y^*)$

We consider parameter τ with a small perturbation δ, i.e., $\tau = \tau^* + \delta$, and then the corresponding characteristic equation can be written as

$$\lambda^2 + p(\delta)\lambda + q(\delta) = 0,$$

where

$$p(\delta) = 2 + (\tau_1{}^* + \delta)(\frac{\Omega - 1}{\Omega^2} - \frac{\alpha r\Omega}{\gamma}),$$

$$q(\delta) = \frac{\Omega r\left[-1 + \Omega\right](\delta + \tau_1{}^*)^2 - r\left(\Omega^2 + (-1 + \Omega)(\tau_1{}^* + \delta)\right)(-\gamma + \Omega r\alpha(\tau_1{}^* + \delta))}{\Omega^2 r\gamma},$$

and the parameter τ_1^* is consistent with the τ_1^* defined in the $N.S$ space.

Since parameters $(\alpha, r, \gamma, \tau) \in N.S$, the roots of the characteristic equation are

$$\lambda_{21,22} = \frac{-p(\delta) \pm i\sqrt{4q(\delta) - p(\delta)^2}}{2},$$

and we have

$$\left|\lambda_{21,22}\right| = \sqrt{q(\delta)} = \sqrt{\frac{\Omega r(-1 + \Omega)(\delta + \tau_1{}^*)^2 - r\left(\Omega^2 + (-1 + \Omega)(\tau_1{}^* + \delta)\right)(-\gamma + \Omega r\alpha(\tau_1{}^* + \delta))}{\Omega^2 r\gamma}},$$

$$\left.\frac{d\left|\lambda_{21,22}\right|}{d\delta}\right|_{\delta=0} = \frac{2\Omega r(-1 + \Omega)\tau_1{}^* - r\left(\Omega^3 r\alpha + \gamma - \Omega\gamma + 2(-1 + \Omega)\Omega r\alpha\tau_1{}^*\right)}{2\Omega^2 r\gamma\sqrt{\frac{\Omega r(-1+\Omega)(\tau_1{}^*)^2 - r\left(\Omega^2 + (-1+\Omega)\tau_1{}^*\right)(-\gamma+\Omega r\alpha\tau_1{}^*)}{\Omega^2 r\gamma}}}.$$

The occurrence of Neimark-Sacker bifurcation requires the following conditions:

(E_1) $\left.\frac{d\left|\lambda_{21,22}\right|}{d\delta}\right|_{\delta=0} \neq 0$;

(E_2) $\lambda_{21,22}^i \neq 1$, when $\delta = 0, i = 1, 2, 3, 4$.

Obviously, (E_1) is identical to the following expression hold:

$$2\Omega r(-1 + \Omega)\tau_1{}^* - r\left(\Omega^3 r\alpha + \gamma - \Omega\gamma + 2(-1 + \Omega)\Omega r\alpha\tau_1{}^*\right) \neq 0,$$

which means that

$$\tau_1{}^* \neq -\frac{\Omega^3 r^2\alpha + r\gamma - \Omega r\gamma}{2\left(-\Omega r^2\alpha + \Omega^2 r^2\alpha - \Omega r(-1+\Omega)\right)}.$$

In addition, (E_2) is identical to $p(0) \neq -2, 0, 1, 2$. Since $|p(0)| < 2$, the condition becomes $p(0) \neq 0, 1$, so we have

$$\tau_1{}^* \neq \frac{2\Omega^2\gamma}{\Omega^3 r\alpha + \gamma - \Omega\gamma}, \text{ and } \tau_1{}^* \neq \frac{\Omega^2\gamma}{\Omega^3 r\alpha + \gamma - \Omega\gamma}.$$

3.2.2. The direction of Neimark-Sacker bifurcation at $E^*(x^*, y^*)$

Let

$$\mu = -\frac{p(0)}{2} = -\frac{2 + \tau_1{}^*(\frac{\Omega-1}{\Omega^2} - \frac{\alpha r\Omega}{\gamma})}{2},$$

$$\omega = \frac{\sqrt{4q(0) - p(0)^2}}{2}$$

$$= \frac{1}{2}\sqrt{-\left(2 + \frac{(-1+\Omega)\,\tau_1{}^*}{\Omega^2} - \frac{\Omega r\alpha\tau_1{}^*}{\gamma}\right)^2 + \frac{4\left(\Omega r(-1+\Omega)(\tau_1{}^*)^2 - r\left(\Omega^2 + (-1+\Omega)\,\tau_1{}^*\right)\left(-\gamma + \Omega r\alpha\tau_1{}^*\right)\right)}{\Omega^2 r\gamma}}.$$

The invertible matrix T_1 can be expressed as

$$T_1 = \begin{pmatrix} \tau_1{}^* r(\Omega - 1) & 0 \\ \mu - 1 - \frac{\tau_1{}^*(\Omega-1)}{\Omega^2} & \omega \end{pmatrix},$$

and its inverse matrix

$$T_1{}^{-1} = \begin{pmatrix} \frac{1}{\tau_1{}^* r(\Omega-1)} & 0 \\ \frac{1-\mu+\frac{\tau_1{}^*(\Omega-1)}{\Omega^2}}{\tau_1{}^* r\omega(\Omega-1)} & \frac{1}{\omega} \end{pmatrix}.$$

We use the following transformation:

$$\begin{pmatrix} \bar{X}_{n+1} \\ \bar{Y}_{n+1} \end{pmatrix} = T_1 \begin{pmatrix} \bar{u}_{n+1} \\ \bar{v}_{n+1} \end{pmatrix},$$

and then the system (3.3) transforms to

$$\begin{pmatrix} \bar{u}_{n+1} \\ \bar{v}_{n+1} \end{pmatrix} = \begin{pmatrix} \mu & -\omega \\ \omega & \mu \end{pmatrix} \begin{pmatrix} \bar{u}_n \\ \bar{v}_n \end{pmatrix} + \tau_1{}^* \begin{pmatrix} f(\bar{X}_n, \bar{Y}_n) \\ g(\bar{X}_n, \bar{Y}_n) \end{pmatrix}, \tag{3.6}$$

where

$$f(\bar{X}_n, \bar{Y}_n) = l_{11}\bar{X}_n^2 + l_{12}\bar{X}_n\bar{Y}_n + l_{13}\bar{Y}_n^2 + l_{14}\bar{X}_n^3 + l_{15}\bar{X}_n^2\bar{Y}_n + l_{16}\bar{X}_n\bar{Y}_n^2 + l_{17}\bar{Y}_n^3 + O((\left|\bar{X}_n\right| + \left|\bar{Y}_n\right|)^4),$$
$$g(\bar{X}_n, \bar{Y}_n) = l_{21}\bar{X}_n^2 + l_{22}\bar{X}_n\bar{Y}_n + l_{23}\bar{Y}_n^2 + l_{24}\bar{X}_n^3 + l_{25}\bar{X}_n^2\bar{Y}_n + l_{26}\bar{X}_n\bar{Y}_n^2 + l_{27}\bar{Y}_n^3 + O((\left|\bar{X}_n\right| + \left|\bar{Y}_n\right|)^4),$$
$$l_{11} = \frac{1}{\tau_1{}^* r(\Omega-1)\Omega^3},\ l_{12} = \frac{1}{\tau_1{}^*(\Omega-1)},\ l_{13} = l_{14} = l_{15} = l_{16} = l_{17} = 0,\ l_{21} = \frac{1-\mu+\frac{\tau_1{}^*(\Omega-1)}{\Omega^2}}{\tau_1{}^* r\omega(\Omega-1)\Omega^3},\ l_{22} = \frac{1-\mu+\frac{\tau_1{}^*(\Omega-1)}{\Omega^2}}{\tau_1{}^*\omega(\Omega-1)} - \frac{1}{\gamma\omega},$$
$$l_{23} = l_{24} = l_{25} = l_{26} = l_{27} = 0.$$

We use the transformation

$$\begin{pmatrix} \bar{X}_n \\ \bar{Y}_n \end{pmatrix} = T_1 \begin{pmatrix} \bar{u}_n \\ \bar{v}_n \end{pmatrix},$$

i.e., $\bar{X}_n = {\tau_1}^* r(\Omega-1)\bar{u}_n,\ \bar{Y}_n = (\mu - 1 - \frac{{\tau_1}^*(\Omega-1)}{\Omega^2})\bar{u}_n + \omega\bar{v}_n$, and then the system (3.6) transforms to

$$\begin{pmatrix} \bar{u}_{n+1} \\ \bar{v}_{n+1} \end{pmatrix} = \begin{pmatrix} \mu & -\omega \\ \omega & \mu \end{pmatrix} \begin{pmatrix} \bar{u}_n \\ \bar{v}_n \end{pmatrix} + {\tau_1}^* \begin{pmatrix} \tilde{f}(\bar{u}_n, \bar{v}_n) \\ \tilde{g}(\bar{u}_n, \bar{v}_n) \end{pmatrix}, \tag{3.7}$$

where

$$\begin{aligned}
&\tilde{f}(\bar{u}_n, \bar{v}_n) = k_{11}\bar{u}_n^2 + k_{12}\bar{u}_n\bar{v}_n + k_{13}\bar{v}_n^2 + k_{14}\bar{u}_n^3 + k_{15}\bar{u}_n^2\bar{v}_n + k_{16}\bar{u}_n\bar{v}_n^2 + k_{17}\bar{v}_n^3 + O((|\bar{u}_n| + |\bar{v}_n|)^4),\\
&\tilde{g}(\bar{u}_n, \bar{v}_n) = k_{21}\bar{u}_n^2 + k_{22}\bar{u}_n\bar{v}_n + k_{23}\bar{v}_n^2 + k_{24}\bar{u}_n^3 + k_{25}\bar{u}_n^2\bar{v}_n + k_{26}\bar{u}_n\bar{v}_n^2 + k_{27}\bar{v}_n^3 + O((|\bar{u}_n| + |\bar{v}_n|)^4),\\
&k_{11} = (-1+\Omega)^2 r^2 {\tau^*}_1^2 l_{11} + (-1+\Omega)\, r{\tau_1}^* \left(-1 + \mu - \tfrac{(-1+\Omega){\tau_1}^*}{\Omega^2}\right) l_{12},\ k_{12} = (-1+\Omega)\, r{\tau_1}^* \omega l_{12},\\
&k_{13} = k_{14} = k_{15} = k_{16} = k_{17} = 0,\ k_{21} = (-1+\Omega)^2 r^2 {\tau^*}_1^2 l_{21} + (-1+\Omega)\, r{\tau_1}^* \left(-1 + \mu - \tfrac{(-1+\Omega){\tau_1}^*}{\Omega^2}\right) l_{22},\\
&k_{22} = (-1+\Omega)\, r{\tau_1}^* \omega l_{22},\ k_{23} = k_{24} = k_{25} = k_{26} = k_{27} = 0.
\end{aligned}$$

To decide the stability of the invariant circle bifurcated from Neimark-Sacker bifurcation of the model (3.7), we are supposed to compute the discriminating coefficient a^*, which is expressed as

$$a^* = -\mathrm{Re}[\frac{(1-2\lambda)\bar{\lambda}^2}{1-\lambda} L_{11}L_{20}] - \frac{1}{2}|L_{11}|^2 - |L_{02}|^2 + \mathrm{Re}(\bar{\lambda}L_{21}),$$

where

$$L_{20} = \frac{1}{8}[(\tilde{f}_{\bar{u}\bar{u}} - \tilde{f}_{\bar{v}\bar{v}} + 2\tilde{g}_{\bar{u}\bar{v}}) + i(\tilde{g}_{\bar{u}\bar{u}} - \tilde{g}_{\bar{v}\bar{v}} - 2\tilde{f}_{\bar{u}\bar{v}})],\ L_{11} = \frac{1}{4}[(\tilde{f}_{\bar{u}\bar{u}} + \tilde{f}_{\bar{v}\bar{v}}) + i(\tilde{g}_{\bar{u}\bar{u}} + \tilde{g}_{\bar{v}\bar{v}})],$$

$$L_{02} = \frac{1}{8}[(\tilde{f}_{\bar{u}\bar{u}} - \tilde{f}_{\bar{v}\bar{v}} - 2\tilde{g}_{\bar{u}\bar{v}}) + i(\tilde{g}_{\bar{u}\bar{u}} - \tilde{g}_{\bar{v}\bar{v}} + 2\tilde{f}_{\bar{u}\bar{v}})],\ L_{21} = \frac{1}{16}[(\tilde{f}_{\bar{u}\bar{u}\bar{u}} + \tilde{f}_{\bar{u}\bar{v}\bar{v}} + \tilde{g}_{\bar{u}\bar{u}\bar{v}} + \tilde{g}_{\bar{v}\bar{v}\bar{v}}) + i(\tilde{g}_{\bar{u}\bar{u}\bar{u}} + \tilde{g}_{\bar{u}\bar{v}\bar{v}} - \tilde{f}_{\bar{u}\bar{u}\bar{v}} - \tilde{f}_{\bar{v}\bar{v}\bar{v}})].$$

Some computations produce that

$$\begin{aligned}
&\tilde{f}_{\bar{u}\bar{u}}\big|_{(0,0)} = 2k_{11},\ \tilde{f}_{\bar{u}\bar{v}}\big|_{(0,0)} = k_{12},\ \tilde{f}_{\bar{u}\bar{u}\bar{u}}\big|_{(0,0)} = 6k_{14},\ \tilde{f}_{\bar{u}\bar{u}\bar{v}}\big|_{(0,0)} = 2k_{15},\ \tilde{f}_{\bar{u}\bar{v}\bar{v}}\big|_{(0,0)} = 2k_{16},\\
&\tilde{f}_{\bar{v}\bar{v}}\big|_{(0,0)} = 2k_{13},\ \tilde{f}_{\bar{v}\bar{v}\bar{v}}\big|_{(0,0)} = 6k_{17},\ \tilde{g}_{\bar{u}\bar{u}}|_{(0,0)} = 2k_{21},\ \tilde{g}_{\bar{u}\bar{v}}|_{(0,0)} = k_{22},\ \tilde{g}_{\bar{u}\bar{u}\bar{u}}|_{(0,0)} = 6k_{24},\\
&\tilde{g}_{\bar{u}\bar{u}\bar{v}}|_{(0,0)} = 2k_{25},\ \tilde{g}_{\bar{u}\bar{v}\bar{v}}|_{(0,0)} = 2k_{26},\ \tilde{g}_{\bar{v}\bar{v}}|_{(0,0)} = 2k_{23},\ \tilde{g}_{\bar{v}\bar{v}\bar{v}}|_{(0,0)} = 6k_{27}.
\end{aligned}$$

Assume that the transversal condition $(E.1)$ and the non-degenerate condition $(E.2)$ of the model (1.3) are satisfied when parameter τ varies in the small region of ${\tau_1}^*$ in the set of $N.S$. The following theorem holds:

Theorem 3.2. *If $a^* \neq 0$, then the system (1.3) undergoes a Neimark-Sacker bifurcation around the positive point $E^*(x^*, y^*)$ when parameter τ fluctuates within the small region of ${\tau_1}^*$ in the set of $N.S$. Furthermore, if $a^* < 0$ (resp., $a^* > 0$), an attracting (resp., repelling) invariant closed curve bifurcates from the point $E^*(x^*, y^*)$ for $\tau > {\tau_1}^*$ (resp., $\tau < {\tau_1}^*$).*

Remark 3.2. *In the discrete mussel-algae system, the biological significance of the Neimark-Sacker bifurcation is that when parameter τ reaches a critical value, the system will change from a stable equilibrium state to a quasi-periodic dynamic, which is represented by periodic oscillations of the population around the equilibrium point. This bifurcation marks an enhancement of nonlinear interactions within the system that may be triggered by environmental changes such as temperature fluctuations, predation conversion rates, mortality, etc.*

3.2.3. Numerical simulation of Neimark-Sacker bifurcation

We choose τ as the bifurcation parameter in parameter space $N.S$. The unique positive equilibrium point $(x_1, y_1) \approx (1.134146341, 0.209183)$ of the model can be obtained by giving the parameters

$$\tau = 1.013343768932,\ \alpha = 0.3,\ r = 2.24,\ \gamma = 5.05.$$

The two eigenvalues of system (1.3) at $E^*(x^*, y^*)$ are $\lambda_{21,22} = 0.982289 \pm 0.187424i$, and by choosing the initial value of $(\tilde{x}_1, \tilde{y}_1) = (1.134, 0.209)$, we can calculate the coefficient $a^*|_{(\tilde{x}_1,\tilde{y}_1)}$ and we have

$$a^*|_{(\tilde{x}_1,\tilde{y}_1)} = -829.405 < 0,$$

so according to Theorem 3.2, model (1.3) undergoes a Neimark-Sacker bifurcation around $(\tilde{x}_1, \tilde{y}_1)$ and bifurcates to an attracting closed invariant curve.

The result can be obtained by numerical simulation as Figures 5 and 6.

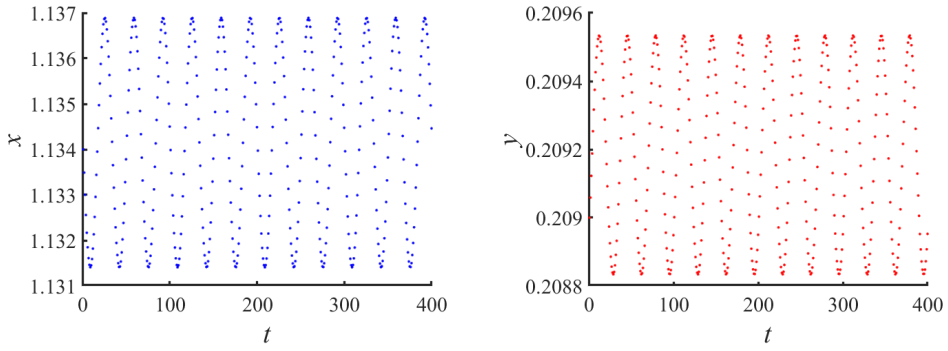

(a) (b)

Figure 5. Neimark-Sacker bifurcation appears around the positive point $(\tilde{x}_1, \tilde{y}_1) = (1.134, 0.209)$. (a) and (b) are the variations of x and y with the time t, respectively.

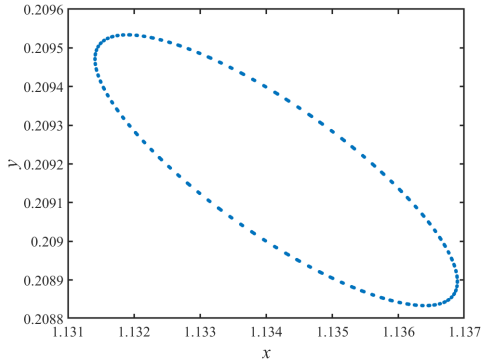

Figure 6. Phase diagrams at the positive point $(\tilde{x}_1, \tilde{y}_1) = (1.134, 0.209)$. There exists an attracting invariant closed curve around the point $(x_1, y_1) \approx (1.134146341, 0.209183)$.

Besides, we choose another set of parameters to consider Neimark-Sacker bifurcation with chaotic cases, that is

$$\tau = 1.39642108,\ \alpha = 0.15,\ r = 2.84,\ \gamma = 1.69.$$

After choosing perturbation parameter $\delta \in (0, 1)$ with step length τ, we can obtain bifurcation diagram and the corresponding maximum Lyapunov exponent (see Figure 7). When the maximum Lyapunov exponent goes from negative to positive, the stability of the system is gradually destroyed and eventually enters a chaotic state within this set of parameters.

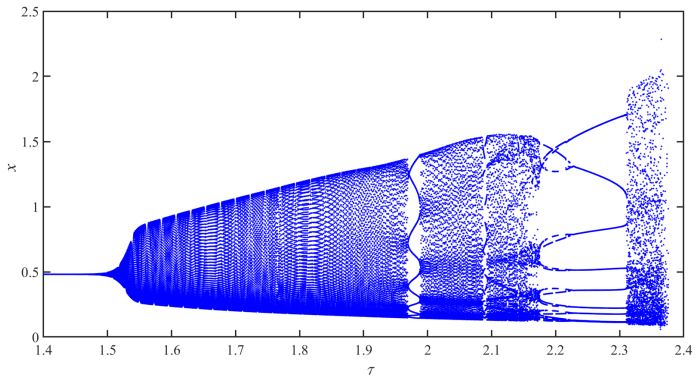

(a)

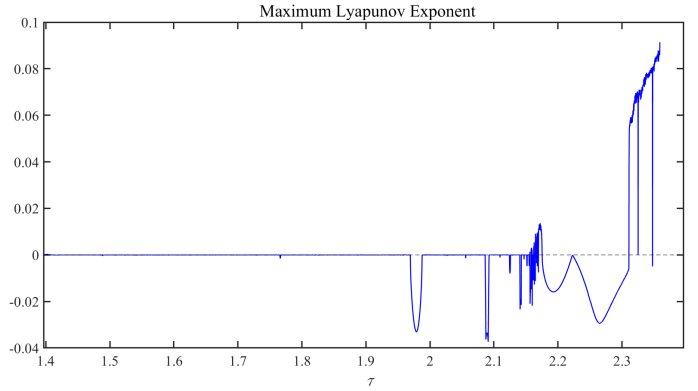

(b)

Figure 7. The bifurcation diagram and the maximum Lyapunov exponent corresponding to perturbation $\delta \in (0, 1)$ with parameter τ for x.

Figure 7 shows that as the bifurcation parameter τ increases, the density of the mussel population gradually starts from the initial stability to the oscillation with increasing amplitude and moves towards chaos.

4. Codimension-two bifurcation analysis

4.1. 1:2 strong resonance

First, we point out how the model (1.3) undergoes 1:2 strong resonance around its unique positive equilibrium point $E^*(x^*, y^*)$ when parameters τ and r are selected as the bifurcation parameters. The

necessary condition for 1:2 strong resonance to occur is determined by the following parameter space:

$$s_{12} = \left\{ H = \frac{G^2}{4}, G \neq 0, \tau = \frac{4}{G} \right\}.$$

In this instance, the critical values of parameters τ and r are represented as ${\tau_2}^*$ and ${r_2}^*$, respectively. The eigenvalues of the matrix $J(E^*)$ are $\lambda_{31,32} = -1$. Let $X_n = x_n - x^*$, $Y_n = y_n - y^*$, which transforms the positive equilibrium $E^*(x^*, y^*)$ to point (0,0) and model (1.3) to

$$\begin{cases} X_{n+1} = X_n + \tau[r(X_n + x^*)(Y_n + y^*) - \frac{X_n + x^*}{1 + X_n + x^*}], \\ Y_{n+1} = Y_n + \frac{\tau}{\gamma}[\alpha(1 - Y_n - y^*) - (X_n + x^*)(Y_n + y^*)], \end{cases} \tag{4.1}$$

and using Taylor expansion at (0,0) yields the following expression:

$$\begin{pmatrix} X_{n+1} \\ Y_{n+1} \end{pmatrix} = \begin{pmatrix} 1 + \frac{\tau(\Omega-1)}{\Omega^2} & \tau r(\Omega - 1) \\ -\frac{\tau}{r\gamma\Omega} & 1 - \frac{\tau\alpha r\Omega}{\gamma} \end{pmatrix} \begin{pmatrix} X_n \\ Y_n \end{pmatrix} + \tau \begin{pmatrix} f(X_n, Y_n) \\ g(X_n, y_n) \end{pmatrix}, \tag{4.2}$$

where

$$f(X_n, Y_n) = \frac{1}{\Omega^3}{X_n}^2 + rX_nY_n - \frac{1}{\Omega^4}{Y_n}^3 + O((|X_n| + |Y_n|)^4), g(X_n, Y_n) = -\frac{1}{\gamma}X_nY_n + O((|X_n| + |Y_n|)^4).$$

We denote $\tilde{J}_1 = J(E^*)|_{({\tau_2}^*, {r_2}^*)}$. The eigenvector and the generalized eigenvector of $\tilde{J}_1$ that correspond to the eigenvalues $\lambda_{31,32} = -1$ are, respectively, $q_{31} = (\tau r(\Omega - 1), -2 - \frac{\tau(\Omega-1)}{\Omega^2})^T$, $p_{32} = (0, 1)^T$, which satisfy $\tilde{J}_1 q_{31} = -q_{31}$, $\tilde{J}_1 q_{32} = -q_{32} + q_{31}$.

Similarly, the eigenvector and the generalized eigenvector of $\tilde{J}_1^T$ are, respectively, $p_{31} = (\frac{1}{\tau r(\Omega-1)}, 0)^T$, $p_{32} = (\frac{1}{\tau r(\Omega-1)}(2 + \frac{\tau(\Omega-1)}{\Omega^2}), 1)^T$, which satisfy $\tilde{J}_1^T p_{32} = -p_{32}$, $\tilde{J}_1^T p_{31} = -p_{31} + p_{32}$.

These four eigenvectors satisfy

$$\langle p_{31}, q_{31} \rangle = \langle p_{32}, q_{32} \rangle = 1, \ \langle p_{31}, q_{32} \rangle = \langle p_{32}, q_{31} \rangle = 0,$$

where $\langle p, q \rangle = \bar{p}_1 q_1 + \bar{p}_2 q_2$ is the standard scalar product in $\mathbb{C}^2$. Therefore, any vectors $(X_n, Y_n)^T$ in $\mathbb{R}^2$ plane can be represented as $(X_n, Y_n)^T = v_{1,n}q_{31} + v_{2,n}q_{32}$. We denote $T_2 = (q_{31}, q_{32})$, then we have

$$\begin{pmatrix} X_n \\ Y_n \end{pmatrix} = T_2 \begin{pmatrix} v_{1,n} \\ v_{2,n} \end{pmatrix},$$

which transforms the system (4.2) to

$$\begin{pmatrix} v_{1,n+1} \\ v_{2,n+1} \end{pmatrix} = \begin{pmatrix} -1 & 1 \\ e_{10}(\tau, r) & -1 + e_{01}(\tau, r) \end{pmatrix} \begin{pmatrix} v_{1,n} \\ v_{2,n} \end{pmatrix} + \begin{pmatrix} f_2(v_{1,n}, v_{2,n}, \tau, r) \\ g_2(v_{1,n}, v_{2,n}, \tau, r) \end{pmatrix}, \tag{4.3}$$

where

$$e_{10}(\tau, r) = \frac{-\alpha(r-1)}{\Omega\gamma}\tau^2 - 2(\frac{\Omega - 1}{\Omega^2} - \frac{\alpha r\Omega}{\gamma})\tau - 4, \ e_{01}(\tau, r) = (\frac{\Omega - 1}{\Omega^2} - \frac{\alpha r\Omega}{\gamma})\tau + 4,$$

$$
\begin{aligned}
f_2(v_{1,n}, v_{2,n}, \tau, r) =&[\frac{\tau^3 r(\Omega-1)}{\Omega^3} + \tau^2 r(-2 - \frac{\tau(\Omega-1)}{\Omega^2})]{v_{1,n}}^2 + \tau^2 r v_{1,n} v_{2,n} - \frac{\tau^4 r^2(\Omega-1)^2}{\Omega^4}{v_{1,n}}^3 \\
&+ O((\left|v_{1,n}\right| + \left|v_{2,n}\right|)^4), \\
g_2(v_{1,n}, v_{2,n}, \tau, r) =&[(2 + \frac{\tau(\Omega-1)}{\Omega^2})(\frac{\tau^3 r(\Omega-1)}{\Omega^3} + \tau^2 r(-2 - \frac{\tau(\Omega-1)}{\Omega^2})) - \frac{\tau^3 r(\Omega-1)}{\gamma}(-2 - \frac{\tau(\Omega-1)}{\Omega^2})]{v_{1,n}}^2 \\
&+ [\tau^2 r(2 + \frac{\tau(\Omega-1)}{\Omega^2}) - \frac{\tau^3 r(\Omega-1)}{\gamma}] v_{1,n} v_{2,n} - \frac{(2 + \frac{\tau(\Omega-1)}{\Omega^2})\tau^4 r^2(\Omega-1)^2}{\Omega^4}{v_{1,n}}^3 \\
&+ O((\left|v_{1,n}\right| + \left|v_{2,n}\right|)^4),
\end{aligned}
$$

and $e_{10}({\tau_2}^*, {r_2}^*) = e_{01}({\tau_2}^*, {r_2}^*) = 0$.

To facilitate description, we denote $\tilde{e}_{10} = e_{10}(\tau, r), \tilde{e}_{01} = e_{01}(\tau, r)$ and $e = (\tilde{e}_{10}, \tilde{e}_{01})^T$, then the system (4.3) can be written as

$$
\begin{pmatrix} v_{1,n+1} \\ v_{2,n+1} \end{pmatrix} = \begin{pmatrix} -1 & 1 \\ \tilde{e}_{10} & -1 + \tilde{e}_{01} \end{pmatrix} \begin{pmatrix} v_{1,n} \\ v_{2,n} \end{pmatrix} + \begin{pmatrix} f_2(v_{1,n}, v_{2,n}, \tau, r) \\ g_2(v_{1,n}, v_{2,n}, \tau, r) \end{pmatrix}, \tag{4.4}
$$

which satisfy $\tilde{e}_{10}({\tau_2}^*, {r_2}^*) = \tilde{e}_{01}({\tau_2}^*, {r_2}^*) = 0$.

Next, we try to simplify the system (4.4) further.

To begin with, we try to use a transformation

$$
\begin{cases}
v_{1,n} = \iota_{1,n} + \sum\limits_{2 \le j+k \le 3} \varphi_{jk}(\tau, r) {\iota_{1,n}}^j {\iota_{2,n}}^k, \\
v_{2,n} = \iota_{2,n} + \sum\limits_{2 \le j+k \le 3} \psi_{jk}(\tau, r) {\iota_{1,n}}^j {\iota_{2,n}}^k,
\end{cases} \tag{4.5}
$$

and its inverse transformation

$$
\begin{cases}
\iota_{1,n} = v_{1,n} - \sum\limits_{j+k=2} \varphi_{jk}(\tau, r) {v_{1,n}}^j {v_{2,n}}^k - \sum\limits_{j+k=3} \alpha_{jk}(\tau, r) {v_{1,n}}^j {v_{2,n}}^k + O((\left|v_{1,n}\right| + \left|v_{2,n}\right|)^4), \\
\iota_{2,n} = v_{2,n} - \sum\limits_{j+k=2} \psi_{jk}(\tau, r) {v_{1,n}}^j {v_{2,n}}^k - \sum\limits_{j+k=3} \beta_{jk}(\tau, r) {v_{1,n}}^j {v_{2,n}}^k + O((\left|v_{1,n}\right| + \left|v_{2,n}\right|)^4),
\end{cases} \tag{4.6}
$$

to remove some higher terms in (4.4), where coefficients φ_{jk} and ψ_{jk} $(2 \le j + k \le 3)$ can be determined later, and coefficients α_{jk} and β_{jk} $(j + k = 3)$ have the following expression:

$$
\begin{aligned}
\alpha_{30} &= \varphi_{30} - 2\varphi_{20}^2 - \varphi_{11}\psi_{20}, \\
\alpha_{21} &= -\varphi_{11}\psi_{11} + \varphi_{21} - 2\varphi_{02}\psi_{20} - 3\varphi_{11}\varphi_{20}, \\
\alpha_{12} &= -2\varphi_{02}\psi_{11} + \varphi_{12} - \varphi_{11}^2 - \varphi_{11}\psi_{02} - 2\varphi_{20}\varphi_{02}, \\
\alpha_{03} &= \varphi_{03} - 2\varphi_{02}\psi_{02} - \varphi_{11}\varphi_{02}, \\
\beta_{30} &= \psi_{30} - 2\psi_{20}\varphi_{20} - \psi_{11}\psi_{20}, \\
\beta_{21} &= -\psi_{11}\varphi_{20} + \psi_{21} - 2\varphi_{11}\psi_{20} - \psi_{11}^2 - 2\psi_{02}\psi_{20}, \\
\beta_{12} &= -\varphi_{11}\psi_{11} + \psi_{12} - 3\psi_{11}\psi_{02} - 2\varphi_{02}\psi_{20}, \\
\beta_{03} &= \psi_{03} - 2\psi_{02}^2 - \varphi_{02}\psi_{11}.
\end{aligned}
$$

By calculation, we can transform system (4.4) to

$$
\begin{pmatrix} \iota_{1,n+1} \\ \iota_{2,n+1} \end{pmatrix} = \begin{pmatrix} -1 & 1 \\ \tilde{e}_{10} & -1 + \tilde{e}_{01} \end{pmatrix} \begin{pmatrix} \iota_{1,n} \\ \iota_{2,n} \end{pmatrix} + \begin{pmatrix} \Psi(\iota_{1,n}, \iota_{2,n}) \\ \Omega(\iota_{1,n}, \iota_{2,n}) \end{pmatrix}, \tag{4.7}
$$

where

$$\Psi(\iota_{1,n},\iota_{2,n}) = \sum_{2\le j+k\le 3} \vartheta_{jk}(\tau,r){\iota_{1,n}}^j{\iota_{2,n}}^k + O((\left|\iota_{1,n}\right| + \left|\iota_{2,n}\right|)^4),$$

$$\Omega(\iota_{1,n},\iota_{2,n}) = \sum_{2\le j+k\le 3} \upsilon_{jk}(\tau,r){\iota_{1,n}}^j{\iota_{2,n}}^k + O((\left|\iota_{1,n}\right| + \left|\iota_{2,n}\right|)^4),$$

here, the specific expressions for ϑ_{ij} and υ_{ij} are given in Appendix C.

In order to eliminate all quadratic terms in (4.4), we let

$$\vartheta_{20} = \vartheta_{11} = \vartheta_{02} = \upsilon_{20} = \upsilon_{11} = \upsilon_{02} = 0,$$

and then the coefficients $\varphi_{jk}(\tau,r)$ and $\psi_{jk}(\tau,r)$ can be obtained for $j+k=2$. We let

$$\vartheta_{30} = \vartheta_{21} = \vartheta_{12} = \vartheta_{03} = \upsilon_{12} = \upsilon_{03} = 0,$$

to eliminate all cubic terms but for resonant ones. This yields equations for $\varphi_{jk}(\tau,r)$ and $\psi_{jk}(\tau,r)$, from which the coefficients $\varphi_{jk}(\tau,r)$ and $\psi_{jk}(\tau,r)$ can be solved for $j+k=3$.

According to the above preparation, we can transform system (4.7) to the normal form of 1:2 resonance under critical condition as follows:

$$\begin{pmatrix} \iota_{1,n+1} \\ \iota_{2,n+1} \end{pmatrix} = \begin{pmatrix} -1 & 1 \\ \tilde{e}_{10} & -1+\tilde{e}_{01} \end{pmatrix}\begin{pmatrix} \iota_{1,n} \\ \iota_{2,n} \end{pmatrix} + \begin{pmatrix} 0 \\ C(\tau,r){\iota_{1,n}}^3 + D(\tau,r){\iota_{1,n}}^2\iota_{2,n} + O((\left|\iota_{1,n}\right| + \left|\iota_{2,n}\right|)^4) \end{pmatrix}, \tag{4.8}$$

where $C(\tau,r) = \upsilon_{30}(\tau,r)$ and $D(\tau,r) = \upsilon_{21}(\tau,r)$. If the parameter τ and r take the critical value ${\tau_2}^*$ and ${r_2}^*$, respectively, then we have

$$\begin{aligned}
\tilde{e}_{10}({\tau_2}^*,{r_2}^*) =& \tilde{e}_{01}({\tau_2}^*,{r_2}^*) = 0,\\
C({\tau_2}^*,{r_2}^*) =& g_{30} + f_{20}g_{20} + \frac{1}{2}{g_{20}}^2 + \frac{1}{2}g_{20}g_{11}\\
=& \frac{1}{2\Omega^{10}\gamma^2}r^2\tau^2(24\Omega^{10}\gamma^2 - 4(-1+\Omega)\Omega^6\gamma\left(4\Omega^4 - \gamma + 8\Omega\gamma - 11\Omega^2\gamma\right)\tau\\
&+ 2(-1+\Omega)^2\Omega^4\left(\Omega^6 + (5-12\Omega)\Omega^3\gamma + (5+\Omega(-19+15\Omega))\gamma^2\right)\tau^2\\
&+ 3(-1+\Omega)^3\Omega^2\left(\Omega^3 + 2\gamma - 3\Omega\gamma\right)\left(\Omega^3 + \gamma - \Omega\gamma\right)\tau^3 + (-1+\Omega)^4\left(\Omega^3 + \gamma - \Omega\gamma\right)^2\tau^4),\\
D({\tau_2}^*,{r_2}^*) =& g_{21} + 3f_{30} + \frac{1}{2}f_{20}g_{11} + \frac{5}{4}g_{20}g_{11} + g_{20}g_{02} + 3{f_{20}}^2 + \frac{5}{2}f_{20}g_{20} + \frac{5}{2}f_{11}g_{20} + {g_{20}}^2 + \frac{1}{2}{g_{11}}^2\\
=& \frac{1}{4\Omega^{10}\gamma^2}r^2\tau^2(112\Omega^{10}\gamma^2 - 4(-1+\Omega)\Omega^6\gamma\left(12\Omega^4 - 3\gamma + 40\Omega\gamma - 49\Omega^2\gamma\right)\tau\\
&+ 8(-1+\Omega)^2\Omega^4\left(\Omega^6 + (5-11\Omega)\Omega^3\gamma + (6+\Omega(-21+16\Omega))\gamma^2\right)\tau^2\\
&+ (-1+\Omega)^3\Omega^2\left(11\Omega^3 + 26\gamma - 37\Omega\gamma\right)\left(\Omega^3 + \gamma - \Omega\gamma\right)\tau^3 + 4(-1+\Omega)^4\left(\Omega^3 + \gamma - \Omega\gamma\right)^2\tau^4).
\end{aligned}$$

We denote the system (4.8) by

$$\iota \mapsto \Gamma_e(\iota),$$

and we can approximate the second iterate ${\Gamma^2}_e(\iota)$ by a flow with the unit-time shift. We point out the map ${\Gamma^2}_e(\iota)$ takes the form

$$\begin{pmatrix} \iota_1 \\ \iota_2 \end{pmatrix} \mapsto \begin{pmatrix} 1+\tilde{e}_{10} & -2+\tilde{e}_{01} \\ -2\tilde{e}_{10} + \tilde{e}_{10}\tilde{e}_{01} & 1+\tilde{e}_{10} - 2\tilde{e}_{01} + \tilde{e}_{01}^2 \end{pmatrix}\begin{pmatrix} \iota_1 \\ \iota_2 \end{pmatrix} + \begin{pmatrix} U(\iota,e) \\ V(\iota,e) \end{pmatrix}, \tag{4.9}$$

where

$$\begin{aligned}U(\iota,e) =&C(\tau,r){\iota_1}^3 + D(\tau,r){\iota_1}^2\iota_2,\\ V(\iota,e) =&(-2C(\tau,r) + \tilde{e}_{10}D(\tau,r) + \tilde{e}_{01}C(\tau,r)){\iota_1}^3 + (3C(\tau,r) - 2D(\tau,r) - 2\tilde{e}_{10}D(\tau,r) + \tilde{e}_{01}D(\tau,r)){\iota_1}^2\iota_2\\ &+ (-3C(\tau,r) + 2D(\tau,r) + \tilde{e}_{10}D(\tau,r) - 2\tilde{e}_{01}D(\tau,r))\iota_1{\iota_2}^2 + (C(\tau,r) - D(\tau,r) + \tilde{e}_{01}D(\tau,r)){\iota_2}^3\\ &+ O((|\iota_1| + |\iota_2|)^4).\end{aligned}$$

For sufficiently small $\|e\|$, the map (4.9) can be approximated by a flow. Using Taylor expansion and solving the following expression:

$$\exp(\wedge_e) = I_2 + \sum_{k=1}\frac{1}{k!}\wedge^k{}_e = \begin{pmatrix} 1+\tilde{e}_{10} & -2+\tilde{e}_{01} \\ -2\tilde{e}_{10}+\tilde{e}_{10}\tilde{e}_{01} & 1+\tilde{e}_{10}-2\tilde{e}_{01}+\tilde{e}_{01}^2 \end{pmatrix},$$

where $\|e\| \neq 0$ is sufficiently small, then we can get

$$\wedge_e = \begin{pmatrix} -\tilde{e}_{10} & -2-\frac{2}{3}\tilde{e}_{10}-\tilde{e}_{01} \\ -2\tilde{e}_{10} & -\tilde{e}_{10}-2\tilde{e}_{01} \end{pmatrix} + O(\|e\|^2).$$

Assume that approximating cubic system $i = \wedge_e\iota + U(\iota,e)$ has the form

$$\begin{pmatrix} i_1 \\ i_2 \end{pmatrix} = \wedge_e\begin{pmatrix} \iota_1 \\ \iota_2 \end{pmatrix} + \begin{pmatrix} p_{30}(e){\iota_1}^3 + p_{21}(e){\iota_1}^2\iota_2 + p_{12}(e)\iota_1{\iota_2}^2 + p_{03}(e){\iota_2}^3 + O((\|\iota_1\| + \|\iota_2\|)^4) \\ q_{30}(e){\iota_1}^3 + q_{21}(e){\iota_1}^2\iota_2 + q_{12}(e)\iota_1{\iota_2}^2 + q_{03}(e){\iota_2}^3 + O((\|\iota_1\| + \|\iota_2\|)^4) \end{pmatrix}, \tag{4.10}$$

where $U(\iota,e)$ is the cubic homogeneous polynomial of ι, in the same time $p_{jk} = p_{jk}(e)$ and $q_{jk} = q_{jk}(e)$ $(j+k=3)$ are undetermined coefficients. For system (4.10), we take three Picard iterations as follows:

$$\begin{aligned}\begin{pmatrix} \iota_1 \\ \iota_2 \end{pmatrix}^{(1)}(\omega) =&\begin{pmatrix} \iota_1 \\ \iota_2 \end{pmatrix}^{(2)}(\omega) = \exp(\wedge_e\omega)\begin{pmatrix} \iota_1 \\ \iota_2 \end{pmatrix}\\ =&\begin{pmatrix} 1-\omega\tilde{e}_{10}+2\omega^2\tilde{e}_{10}+O(\|e\|^2) & -\omega(2+\frac{3}{2}\tilde{e}_{10}+\tilde{e}_{01})+2\omega^2(\tilde{e}_{10}+\tilde{e}_{01})+O(\|e\|^2) \\ -2\omega\tilde{e}_{10}+O(\|e\|^2) & 1-\omega(\tilde{e}_{10}+2\tilde{e}_{01})+2\omega^2\tilde{e}_{10}+O(\|e\|^2) \end{pmatrix}\begin{pmatrix} \iota_1 \\ \iota_2 \end{pmatrix},\\ \begin{pmatrix} \iota_1 \\ \iota_2 \end{pmatrix}^{(3)}(\omega) =&\exp(\wedge_e\omega)\begin{pmatrix} \iota_1 \\ \iota_2 \end{pmatrix} + \int_0^\omega \exp(\wedge_e(\omega-t))(F^{(2)}({\iota_1}^{(2)},{\iota_2}^{(2)}) + F^{(3)}({\iota_1}^{(2)},{\iota_2}^{(2)}))dt,\end{aligned}$$

where $F^{(2)}({\iota_1}^{(2)},{\iota_2}^{(2)})$ and $F^{(3)}({\iota_1}^{(2)},{\iota_2}^{(2)})$ are smooth quadratic and cubic polynomial functions on ${\iota_1}^{(2)}$, ${\iota_2}^{(2)}$, respectively.

Taking the valve $\omega = 1$, then we get

$$\begin{pmatrix} \iota_1 \\ \iota_2 \end{pmatrix}^{(3)}(1) =$$

$$\begin{pmatrix} (1+\tilde{e}_{10})\iota_1 + (-2+\tilde{e}_{01})\iota_2 + c_{30}{\iota_1}^3 + c_{21}{\iota_1}^2\iota_2 + c_{12}\iota_1{\iota_2}^2 + c_{03}{\iota_2}^3 + O((\|\iota_1\| + \|\iota_2\|)^4) \\ (-2\tilde{e}_{10}+\tilde{e}_{10}\tilde{e}_{01})\iota_1 + (1+\tilde{e}_{10}-2\tilde{e}_{01}+\tilde{e}_{01}^2)\iota_2 + d_{30}{\iota_1}^3 + d_{21}{\iota_1}^2\iota_2 + d_{12}\iota_1{\iota_2}^2 + d_{03}{\iota_2}^3 + O((\|\iota_1\| + \|\iota_2\|)^4) \end{pmatrix},$$

where

$$\begin{aligned}&c_{30} = p_{30} - q_{30},\ c_{21} = -3p_{30} + p_{21} + 2q_{30} - q_{21},\ c_{12} = 4p_{30} - 2p_{21} + p_{12} - 2q_{30} + \tfrac{4}{3}q_{21} - q_{12},\\ &c_{03} = -2p_{30} + \tfrac{4}{3}p_{21} - p_{12} + p_{03} + \tfrac{4}{5}q_{30} - \tfrac{2}{3}(q_{21} - q_{12}) - q_{03},\ d_{30} = q_{30}, d_{21} = -3q_{30} + q_{21},\\ &d_{12} = 4q_{30} - 2q_{21} + q_{12},\ d_{03} = -2q_{30} + \tfrac{4}{3}q_{21} - q_{12} + q_{03}.\end{aligned}$$

Solving the equation for p_{jk} and q_{jk} and applying it to (4.9), we obtain

$$p_{30} = -C(\tau, r),\ p_{21} = -2C(\tau, r) - D(\tau, r),\ p_{12} = -C(\tau, r) - \tfrac{4}{3}D(\tau, r),\ p_{03} = -\tfrac{1}{15}C(\tau, r) - \tfrac{1}{3}D(\tau, r),$$
$$q_{30} = -2C(\tau, r),\ q_{21} = -3C(\tau, r) - 2D(\tau, r),\ q_{12} = -C(\tau, r) - 2D(\tau, r),\ q_{03} = -\tfrac{1}{3}D(\tau, r).$$

Therefore, the undetermined coefficients in system (4.10) are obtained and the system (4.9) can be represented as

$$\Gamma_e{}^2(\iota) = \varphi_e{}^1 + O(\|\iota\|^4),$$

where $\varphi_e{}^1$ is the flow of the system (4.10) and $\|e\|$ is sufficiently small.

Using a transformation, we can simplify (4.10) further.

Let

$$\begin{cases} \chi_1 = \iota_1 + (\frac{1}{6}p_{12}(e) + \frac{1}{12}q_{12}(e))\iota_1{}^3 + (\frac{1}{4}p_{12}(e) + \frac{1}{4}q_{03}(e))\iota_1{}^2\iota_2 + \frac{1}{2}p_{03}(e)\iota_1\iota_2{}^2, \\ \chi_2 = -\tilde{e}_{10}\iota_1 - (2 + \frac{2}{3}\tilde{e}_{10} + \tilde{e}_{01})\iota_2 + p_{30}(e)\iota_1{}^3 - \frac{1}{2}q_{12}(e)\iota_1{}^2\iota_2 - q_{03}(e)\iota_1\iota_2{}^2, \end{cases}$$

and then the system (4.10) becomes as

$$\begin{pmatrix} \dot{\chi}_1 \\ \dot{\chi}_2 \end{pmatrix} = \begin{pmatrix} 0 & 1 \\ 4\tilde{e}_{10} + O(\|e\|^2) & -2\tilde{e}_{10} - 2\tilde{e}_{01} + O(\|e\|^2) \end{pmatrix} \begin{pmatrix} \chi_1 \\ \chi_2 \end{pmatrix} + \begin{pmatrix} 0 \\ C_1(e)\chi_1{}^3 + D_1(e)\chi_1{}^2\chi_2 \end{pmatrix}, \tag{4.11}$$

where $C_1(e)$ and $C_2(e)$ satisfy

$$C_1(\tau_2{}^*, r_2{}^*) = 4C(\tau_2{}^*, r_2{}^*), D_1(\tau_2{}^*, r_2{}^*) = -2D(\tau_2{}^*, r_2{}^*) - 6C(\tau_2{}^*, r_2{}^*).$$

According to Theorem 9.3 in [23], we know that the second iteration of (4.8) can be smoothly equivalent to the system (4.11), so all we need to do is study the properties of approximating system (4.11).

In the following, we suppose that nondegeneracy conditions hold:

$$C_1(\tau_2{}^*, r_2{}^*) \neq 0, D_1(\tau_2{}^*, r_2{}^*) \neq 0, \tag{4.12}$$

which is equivalent to $C(\tau_2{}^*, r_2{}^*) \neq 0, D(\tau_2{}^*, r_2{}^*) + 3C(\tau_2{}^*, r_2{}^*) \neq 0$.

Assuming $D_1(\tau_2{}^*, r_2{}^*) < 0$, (or else, reversing time and taking $\chi \mapsto -\chi$) and we can let

$$\eta_1 = \frac{-D_1(e)}{\sqrt{\sigma C_1(e)}}\chi_1,\ \eta_2 = \frac{D_1{}^2(e)}{C_1(e)\sqrt{\sigma C_1(e)}}\chi_2,\ t = -\frac{C_1(e)}{D_1(e)}\tau,$$

where $\sigma = \pm 1$ and $\sigma = 1$ for $C_1(\tau_2{}^*, r_2{}^*) > 0$, then the system (4.11) can become as

$$\begin{cases} \dot{\eta}_1 = \eta_2, \\ \dot{\eta}_2 = \varsigma_1\eta_1 + \varsigma_2\eta_2 + \sigma\eta_1{}^3 - \eta_1{}^2\eta_2, \end{cases} \tag{4.13}$$

where $\varsigma_1 = (4\tilde{e}_{10} + O(\|e\|^2))\frac{D_1{}^2(e)}{C_1{}^2(e)}$, $\varsigma_2 = 2(\tilde{e}_{10} + \tilde{e}_{01} + O(\|e\|^2))\frac{D_1(e)}{C_1(e)}$, $\sigma = \pm 1$ and $\sigma = 1$ for $C_1(\tau_2{}^*, r_2{}^*) > 0$.

Finally, the following theorem is obtained according to relevant research results [23].

Theorem 4.1. *If (4.12) and the condition $(A_4)(i)$ in Lemma 2.1 are both met, the model (1.3) will experience 1:2 strong resonance at $E^*(x^*, y^*)$. Furthermore, model (1.3) exhibits the following bifurcation behavior in a small neighborhood of s_{12} near $E^*(x^*, y^*)$:*

(1) A Flip bifurcation curve may exist: $FL = \{(\varsigma_1, \varsigma_2)|\varsigma_1 = 0\}$ *. A stable periodic-2 cycle emerges from* $E^*(x^*, y^*)$ *once crossing the curve.*

(2) A nondegenerate Neimark-Sacker bifurcation curve may exist: $NS = \{(\varsigma_1, \varsigma_2)|\varsigma_2 = 0, \varsigma_1 < 0\}$ *. A stable closed invariant cycle occurs and surrounds the fixed point* $E^*(x^*, y^*)$ *as it crosses the curve.*

(3) A homoclinic structure exists, which indicates the presence of long-period cycles that emerge and disappear through fold bifurcations within an exponentially narrow parameter region around $CH = \left\{(\varsigma_1, \varsigma_2)|\varsigma_2 = -\frac{1}{5}\varsigma_1 + O(\varsigma_1), \varsigma_1 < 0\right\}$.

4.2. 1:3 strong resonance

In this section, parameters τ and r are selected as the bifurcation parameters to investigate the 1:3 strong resonance bifurcation of system (1.3) at the positive equilibrium point $E^*(x^*, y^*)$. This bifurcation occurs when τ and r fluctuate within a narrow area of s_{13}, where

$$s_{13} = \left\{H = \frac{G^2}{3}, G \neq 0, \tau = \frac{3}{G}\right\}.$$

The critical values for τ and r are denoted by the notations ${\tau_3}^*$ and ${r_3}^*$, respectively. Regarding $J(E^*)$, its two eigenvalues are $\lambda_{41,42} = \frac{-1\pm\sqrt{3}i}{2}$. Just like in the case of the 1:2 resonance, we transform the positive equilibrium $E^*(x^*, y^*)$ into $(0, 0)$ and expand the right side of model (1.3):

$$\begin{pmatrix} X_{n+1} \\ Y_{n+1} \end{pmatrix} = \begin{pmatrix} 1 + \frac{\tau(\Omega-1)}{\Omega^2} & \tau r(\Omega - 1) \\ -\frac{\tau}{r\gamma\Omega} & 1 - \frac{\tau\alpha r\Omega}{\gamma} \end{pmatrix} \begin{pmatrix} X_n \\ Y_n \end{pmatrix} + \tau \begin{pmatrix} f(X_n, Y_n) \\ g(X_n, y_n) \end{pmatrix}, \tag{4.14}$$

where $f(X_n, Y_n)$ and $g(X_n, Y_n)$ are the same as that of (4.2).

We denote $J(E^*) = \begin{pmatrix} 1 + \frac{\tau(\Omega-1)}{\Omega^2} & \tau r(\Omega - 1) \\ -\frac{\tau}{r\gamma\Omega} & 1 - \frac{\tau\alpha r\Omega}{\gamma} \end{pmatrix}$, and $\tilde{J}_2 = J|_{({\tau_3}^*, {r_3}^*)}$. The eigenvector of $\tilde{J}_2$ corresponding to the eigenvalue $\lambda_{41} = \frac{-1+\sqrt{3}i}{2}$ is $q_4 = (q_{41}, q_{42})^T = (\tau r(\Omega - 1), -1 - \frac{\tau(\Omega-1)}{\Omega^2} - \frac{1-\sqrt{3}i}{2})^T$, which satisfies $\tilde{J}_2 q_4 = \lambda_{41} q_4$. Similarly, the eigenvector of $\tilde{J}_2^T$ corresponding to the eigenvalue $\lambda_{42} = \frac{-1-\sqrt{3}i}{2}$ is $p_4 = (p_{41}, p_{42})^T = (\frac{\sqrt{3}i(3+\frac{2\tau(\Omega-1)}{\Omega^2})+3}{6\tau r(\Omega-1)}, \frac{\sqrt{3}i}{3})^T$, which satisfies $\tilde{J}_2^T p_4 = \lambda_{42} p_4$, and $\langle p_4, q_4\rangle = 1$, where $\langle ., .\rangle$ represents the standard scalar product in $\mathbb{C}^2$.

Thus, every vector $(X_n, Y_n)^T \in \mathbb{R}^2$ can be represented in the form $(X_n, Y_n)^T = zq_4 + \bar{z}\bar{q}_4$. Therefore, system (4.14) can be expressed as the complex form as follows:

$$\begin{pmatrix} z(n+1) \\ \bar{z}(n+1) \end{pmatrix} = \begin{pmatrix} \lambda_{41} & 0 \\ 0 & \bar{\lambda}_{41} \end{pmatrix} \begin{pmatrix} z(n) \\ \bar{z}(n) \end{pmatrix} + \begin{pmatrix} \sum\limits_{2\le i+j\le 3} g_{ij} z^i(n)\bar{z}^j(n) + O(\|(z(n), \bar{z}(n)\|^4) \\ \sum\limits_{2\le i+j\le 3} \bar{g}_{ij} z^i(n)\bar{z}^j(n) + O(\|(z(n), \bar{z}(n)\|^4) \end{pmatrix}, \tag{4.15}$$

where

$$\begin{aligned} &g_{20} = \tau(\bar{p}_{41} + \bar{p}_{42})(\tfrac{1}{\Omega^3}{q^2}_{41} + rq_{41}q_{42}), g_{11} = \tau(\bar{p}_{41} + \bar{p}_{42})(rq_{41}\bar{q}_{42} + r\bar{q}_{41}q_{42} + \tfrac{2}{\Omega^3}q_{41}\bar{q}_{41}),\\ &g_{02} = \tau(\bar{p}_{41} + \bar{p}_{42})(r\bar{q}_{41}\bar{q}_{42} + \tfrac{1}{\Omega^3}\bar{q}^2_{41}), g_{30} = \tau(\bar{p}_{41} + \bar{p}_{42})(-\tfrac{1}{\Omega^4}{q^3}_{42}), g_{21} = \tau(\bar{p}_{41} + \bar{p}_{42})(-\tfrac{3}{\Omega^4}{q^2}_{42}\bar{q}_{42}),\\ &g_{12} = \tau(\bar{p}_{41} + \bar{p}_{42})(-\tfrac{3}{\Omega^4}q_{42}\bar{q}^2_{42}), g_{03} = \tau(\bar{p}_{41} + \bar{p}_{42})(-\tfrac{1}{\Omega^4}\bar{q}^3_{42}), \end{aligned}$$

and $\bar{g}_{ij}$ is the complex conjugate of g_{ij}.

Since the component of (4.15) can be seen as the real part and the corresponding complex conjugate part, we need only study the following expression:

$$z(n+1) = \lambda_{41} z(n) + \sum_{2\le i+j\le 3} g_{ij} z^i(n)\bar{z}^j(n) + O(\|z(n), \bar{z}(n)\|^4). \tag{4.16}$$

Using the following transformation:

$$z(n) = \phi(n) + \frac{\sigma_{20}}{2}\phi^2(n) + \sigma_{11}\phi(n)\bar{\phi}(n) + \frac{\sigma_{02}}{2}\bar{\phi}^2(n), \tag{4.17}$$

and its inverse transformation

$$\begin{aligned}\phi(n) = {} & z(n) - \frac{\sigma_{20}}{2}z^2(n) - \sigma_{11}z(n)\bar{z}(n) - \frac{\sigma_{02}}{2}\bar{z}^2(n)\\ & + \frac{1}{2}(\sigma_{20}^2 + \sigma_{11}\bar{\sigma}_{02})z^3(n) + \left(|\sigma_{11}|^2 + \frac{3}{2}\sigma_{11}\sigma_{20} + \frac{1}{2}|\sigma_{02}|^2\right)z^2(n)\bar{z}(n)\\ & + \left(\frac{1}{2}\sigma_{11}\bar{\sigma}_{20} + \sigma_{11}^2 + \sigma_{02}\bar{\sigma}_{11} + \frac{1}{2}\sigma_{02}\sigma_{20}\right)z(n)\bar{z}^2(n)\\ & + \frac{1}{2}(\sigma_{02}\bar{\sigma}_{20} + \sigma_{11}\sigma_{02})\bar{z}^3(n) + O(\|z(n), \bar{z}(n)\|^4),\end{aligned} \tag{4.18}$$

where coefficients σ_{20}, σ_{11} and σ_{02} are undetermined, then we can eliminate several quadratic terms in (4.16), which is transformed into

$$\phi(n+1) = \lambda_{41}\phi(n) + \sum_{2\le i+j\le 3} \tilde{\sigma}_{ij}\phi^i(n)\,\bar{\phi}^j(n) + O(\left\|(\phi(n), \bar{\phi}(n))\right\|^4), \tag{4.19}$$

where $\tilde{\sigma}_{ij}$ are given in Appendix D.

By setting

$$\sigma_{20} = \frac{2\sqrt{3}i}{3}g_{20},\ \sigma_{11} = \frac{3+\sqrt{3}i}{6}g_{11},\ \sigma_{02} = 0,$$

then the coefficients in (4.17) are well defined, and the system (4.19) can be reduced as follows:

$$\phi(n+1) = \lambda_{41}\phi(n) + g_{02}\bar{\phi}^2(n) + \sum_{i+j=3} \tilde{\sigma}_{ij}\phi^i(n)\,\bar{\phi}^j(n) + O(\left\|(\phi(n), \bar{\phi}(n))\right\|^4). \tag{4.20}$$

In order to remove certain cubic terms, we perform the following transformation:

$$\phi(n) = \eta(n) + \frac{\sigma_{30}}{6}\eta^3(n) + \frac{\sigma_{21}}{2}\eta^2(n)\bar{\eta}(n) + \frac{\sigma_{12}}{2}\eta(n)\bar{\eta}^2(n) + \frac{\sigma_{03}}{6}\bar{\eta}^3(n), \tag{4.21}$$

and its inverse transformation

$$\eta(n) = \phi(n) - \frac{\sigma_{30}}{6}\phi^3(n) - \frac{\sigma_{21}}{2}\phi^2(n)\,\bar{\phi}(n) - \frac{\sigma_{12}}{2}\phi(n)\,\bar{\phi}^2(n) - \frac{\sigma_{03}}{6}\bar{\phi}^3(n) + O(\left\|(\phi(n), \bar{\phi}(n))\right\|^4), \tag{4.22}$$

and then system (4.20) becomes

$$\eta(n+1) = \lambda_{41}\eta(n) + g_{02}\bar{\eta}^2(n) + \sum_{i+j=3} h_{ij}\eta^i(n)\bar{\eta}^j(n) + O(\|(\eta(n), \bar{\eta}(n))\|^4), \tag{4.23}$$

where

$$h_{30} = \tilde{\sigma}_{30} + \frac{\sqrt{3}i - 3}{12}\sigma_{30},\ h_{21} = \tilde{\sigma}_{21},\ h_{12} = \tilde{\sigma}_{12} + \frac{\sqrt{3}i}{2}\sigma_{12},\ h_{03} = \tilde{\sigma}_{03} + \frac{\sqrt{3}i - 3}{12}\sigma_{03}.$$

By taking

$$\sigma_{30} = (3 + \sqrt{3}i)\tilde{\sigma}_{30},\ \sigma_{21} = 0,\ \sigma_{12} = \frac{2\sqrt{3}i}{3}\tilde{\sigma}_{12},\ \sigma_{03} = (3 + \sqrt{3}i)\tilde{\sigma}_{03},$$

we can eliminate the coefficients in front of the cubic terms $\eta^3, \eta\bar{\eta}^2$ and $\bar{\eta}^3$, and system (4.23) can be reduced into

$$\eta(n+1) = \lambda_{41}\eta(n) + g_{02}\bar{\eta}^2(n) + h_{21}\eta^2(n)\,\bar{\eta}(n) + O(\|(\eta(n), \bar{\eta}(n))\|^4). \tag{4.24}$$

We define

$$\begin{aligned} \rho_1 &= -\tfrac{3+3\sqrt{3}i}{2} g_{02}, \\ \rho_2 &= -\tfrac{3+3\sqrt{3}i}{2} h_{21} - 3|g_{02}|^2, \end{aligned}$$

according to the relevant research results [23], the following theorem can be derived.

Theorem 4.2. *If $\rho_1 \neq 0$, $\mathrm{Re}(\rho_2) \neq 0$, and the condition $(A_4)(ii)$ of Lemma 2.1 are both met, the model (1.3) will experience 1:3 strong resonance at $E^*(x^*, y^*)$. The expression $\mathrm{Re}(\rho_2) \neq 0$ determines the stability of the invariant closed curve. Futhermore, model (1.3) exhibits the following bifurcation behavior in a small region of s_{13} near $E^*(x^*, y^*)$:*

(1) A nondegenerate Neimark-Sacker bifurcation curve may exist around the trivial fixed point $E^*(x^*, y^*)$.

(2) A saddle cycle of 3-period may occur surrounding the saddle fixed point $E^*(x^*, y^*)$.

(3) A homoclinic structure occurs when the stable and unstable invariant manifolds of a period three cycle interact transversally within a parameter region, which is exponentially narrow.

4.3. 1:4 strong resonance

In this subsection, we study 1:4 strong resonance bifurcation of model (1.3) around its unique positive equilibrium point $E^*(x^*, y^*)$ when parameters τ and r are selected as the bifurcation parameters. The necessary condition for 1:4 strong resonance to occur is determined by the following parameter space:

$$s_{14} = \left\{ H = \frac{G^2}{2}, G \neq 0, \tau = \frac{2}{G} \right\}.$$

Now, the critical values of parameters τ and r are represented as ${\tau_4}^*$ and ${r_4}^*$, respectively. The eigenvalues of the matrix $J(E^*)$ are $\lambda_{51,52} = \pm i$. Similar to the 1:2 and 1:3 resonance cases, we transform the positive equilibrium $E^*(x^*, y^*)$ into $(0, 0)$ and expand the right side of model (1.3), and the Jacobian matrix evaluated at the fixed point $E^*(x^*, y^*)$ is

$$J(E^*) = \begin{pmatrix} 1 + \frac{\tau(\Omega-1)}{\Omega^2} & \tau r(\Omega - 1) \\ -\frac{\tau}{r\gamma\Omega} & 1 - \frac{\tau\alpha r\Omega}{\gamma} \end{pmatrix},$$

and we denote $J_0 = J|_{(\tau_4^*, r_4^*)}$.

The eigenvector of J_0 corresponding to the eigenvalue $\lambda_{51} = i$ is $q_5 = (q_{51}, q_{52})^T = (\tau r(\Omega - 1), -1 - \frac{\tau(\Omega-1)}{\Omega^2} + i)^T$, which satisfies $J_0 q_5 = \lambda_{51} q_5$. Similarly, the eigenvector of ${J_0}^T$ corresponding to the eigenvalue $\lambda_{52} = -i$ is $p_5 = (p_{51}, p_{52})^T = (\frac{-1+(1+\frac{\tau(\Omega-1)}{\Omega^2})i}{2\tau r(\Omega-1)}, \frac{i}{2})^T$, which satisfies ${J_0}^T p_5 = \lambda_{52} p_5$, and $\langle p_5, q_5 \rangle = 1$, in which $\langle ., . \rangle$ is the standard scalar product in $\mathbb{C}^2$.

Thus, each vector $(X_n, Y_n)^T \in \mathbb{R}^2$ can be represented in the form $(X_n, Y_n)^T = z q_5 + \bar{z}\bar{q}_5$. Therefore, the model (4.2) can be expressed as the complex form as follows:

$$z(n+1) = \lambda_{51} z(n) + \sum_{2 \le i+j \le 3} g_{ij} z^i(n) \bar{z}^i(n) + O(\|(z(n), \bar{z}(n))\|^4), \tag{4.25}$$

where g_{ij} $(2 \le i + j \le 3)$ are determined according to (4.15) with the terms p_{4i}, q_{4i} $(i = 1, 2)$ being substituted by p_{5i}, q_{5i} $(i = 1, 2)$, respectively.

Taking transformations which is similar to 1:3 resonance case, finally we transform system (4.25) into the following form:

$$\phi(n+1) = \lambda_{51} \phi(n) + \sum_{2 \le i+j \le 3} \tilde{\sigma}_{ij} \phi^i(n) \bar{\phi}^j(n) + O(\left\|(\phi(n), \bar{\phi}(n))\right\|^4), \tag{4.26}$$

where $\tilde{\sigma}_{ij}$ are given in Appendix E.

Subsequently, we require to remove certain quadratic and cubic terms in (4.26) using the identical approach as the 1:3 scenario. Employing the same transformation and its inverse transformation (see (4.17) and (4.18) in Section 4.2), the system (4.26) can be reduced.

Let

$$\sigma_{20} = (i-1) g_{20},\ \sigma_{11} = \frac{1+i}{2} g_{11},\ \sigma_{02} = (i-1) g_{02},$$

then the quadratic terms can be removed and the system (4.26) becomes

$$\phi(n+1) = \lambda_{51} \phi(n) + \sum_{i+j=3} \tilde{\sigma}_{ij} \phi^i(n) \bar{\phi}^j(n) + O(\left\|(\phi(n), \bar{\phi}(n))\right\|^4). \tag{4.27}$$

Furthermore, after taking the transformation (4.21) and (4.22) in Section 4.2, system (4.27) can be transformed into:

$$\eta(n+1) = \lambda_{51} \eta(n) + \sum_{i+j=3} h_{ij} \eta^i(n) \bar{\eta}^j(n) + O(\|(\eta(n), \bar{\eta}(n))\|^4), \tag{4.28}$$

where

$$h_{30} = \tilde{\sigma}_{30} + \frac{i}{3}\sigma_{30},\ h_{21} = \tilde{\sigma}_{21},\ h_{12} = \tilde{\sigma}_{12} + i\sigma_{12},\ h_{03} = \tilde{\sigma}_{03}.$$

By setting

$$\sigma_{30} = 3i\tilde{\sigma}_{30},\ \sigma_{21} = 0,\ \sigma_{12} = i\tilde{\sigma}_{12},\ \sigma_{03} = 0,$$

we have $h_{30} = h_{12} = 0$, and then system (4.28) can be finally simplified as follows:

$$\eta(n+1) = \lambda_{51} \eta(n) + h_{21} \eta^2(n) \bar{\eta}(n) + h_{03} \bar{\eta}^3(n) + O(\|(\eta(n), \bar{\eta}(n))\|^4). \tag{4.29}$$

Define the two quantities

$$\mu_1 = -2h_{21}i, \ \ \mu_2 = -\frac{2}{3}h_{03}i,$$

if $\mu_2 \neq 0$, we may write $\mu_3 = \frac{\mu_1}{|\mu_2|}$. According to the relevant research results [23], the following theorem can be derived.

Theorem 4.3. *If $\mu_2 \neq 0$, $\mathrm{Re}(\mu_3) \neq 0$, $\mathrm{Im}(\mu_3) \neq 0$ and the condition $(A_4)(iii)$ of Lemma 2.1 are both satisfied, model (1.3) will experience 1:4 strong resonance at $E^*(x^*, y^*)$. The expression μ_3 determines different bifurcation situations around the equilibrium $E^*(x^*, y^*)$. There are two-parameter families of equilibria that undergo a fourth-order bifurcation from $E^*(x^*, y^*)$. One can be either unstable, attracting, or repelling invariant closed curves, depending on the values chosen for the parameters τ and r. Furthermore, in a sufficiently narrow region of s_{14} around the point $E^*(x^*, y^*)$, there exist several complicated bifurcation curves of codimension-one of map (4.29).*

Remark 4.1. *In biological systems, these codimension-two bifurcations (1:2, 1:3, and 1:4 strong resonances) elucidate the intricate dynamics of mussel-algae interactions. These strong resonance bifurcations can trigger periodic drastic fluctuations in mussel and algal populations. Furthermore, initially stable periodic regimes may transition to complex behaviors such as period-doubling cascades or chaos, thereby destabilizing the ecosystem of both populations.*

4.4. Numerical simulations of codimension two bifurcations

In this work, we conduct several numerical simulations for analyzing the system (1.3). Results of these simulations can be presented in various forms, such as bifurcation diagrams, maximal Lyapunov exponents, and phase portraits. In addition, new dynamical behaviors revealed by these figures also verify the theoretical analysis above.

4.4.1. Numerical simulation of 1:2 resonance

Fix parameters $\alpha = 0.305$, $\gamma = 0.56$. The critical parameter values are ${\tau_2}^* = 4.100684389917548$, ${r_2}^* = 1.589$ and model (1.3) has a positive equilibrium point $E^*(x^*, y^*) = (0.348584956001203, 0.466657007936759)$. Further calculations result in $\lambda_{31,32} = -1$, $C({\tau_2}^*, {r_2}^*) = -83.9310477 \neq 0$ and $D({\tau_2}^*, {r_2}^*) = 265.49693657 \neq 0$. From Theorem 4.1 we can conclude that system (1.3) will undergo a 1:2 strong resonance bifurcation around $E^*(x^*, y^*)$.

Figure 8 illustrates a three-dimensional bifurcation diagram in the (τ, r, x) plane around $E^*(x^*, y^*)$ when parameters τ and r fluctuate within a small region around $({\tau_2}^*, {r_2}^*) = (4.100684389917548, 1.589)$. Figure 9(a) depicts a two-dimension bifurcation diagram in (τ, x) space when $r = {r_2}^* = 1.589$ and τ fluctuates within the range $[4.05, 4.32]$. Figure 9(b) displays the maximum Lyapunov exponents associated with Figure 9(a). It reveals the existence of stable fixed points or stable periodic windows within the chaotic region. In this region, some of the maximum Lyapunov exponents are positive while others are negative.

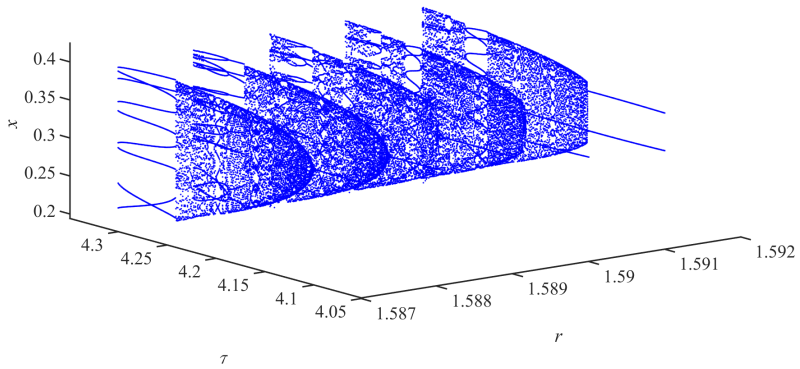

Figure 8. The three-dimensional bifurcation diagram in the (τ, r, x)-space shows the variations when the variables τ and r varied. The parameter r takes on the values 1.587, 1.588, 1.589, 1.590, 1.591 from left to right.

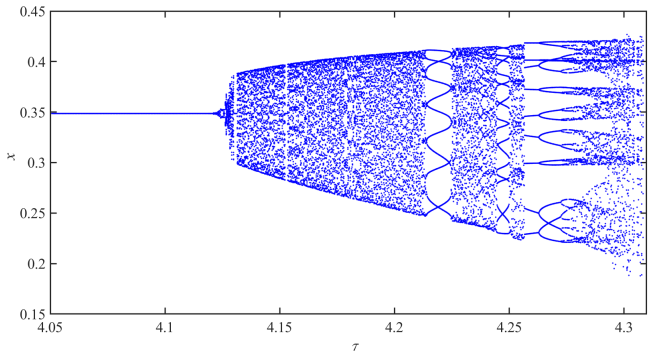

(a)

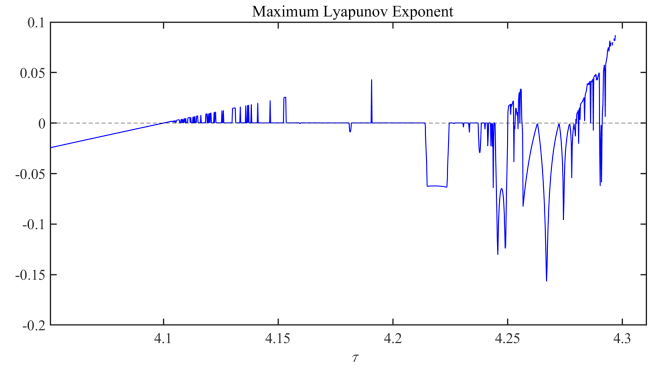

(b)

Figure 9. (a) The bifurcation diagram when a 1:2 strong resonance occurs in (τ, x)-space with $r = 1.589$ and $\tau \in [4.05, 4.32]$. (b) The Maximum Lyapunov exponents associated with (a).

Figure 10(a)–(g) shows the phase portraits of system (1.3) around the fixed point $E^*(x^*, y^*)$ with different parameters τ and r. When taking the parameters $\tau = 4.100684389917548$, $r = 1.551$,

a Neimark-Sacker bifurcation occurs resulting in the appearance of an invariant limit cycle from $E^*(x^*, y^*)$. Figure 10(c) depicts the invariant limit cycle. Besides, Stable closed invariant curve for $\tau = 4.114184389917548$ and $r = 1.58$ can be seen in Figure 10(d). A period-80 curve occurs at the parameters $\tau = 4.240684389917548$ and $r = 1.58$, which is shown in Figure 10(e). In Figure 10(f), chaotic behavior occurs when $\tau = 4.314884389917548$ and $r = 1.551$.

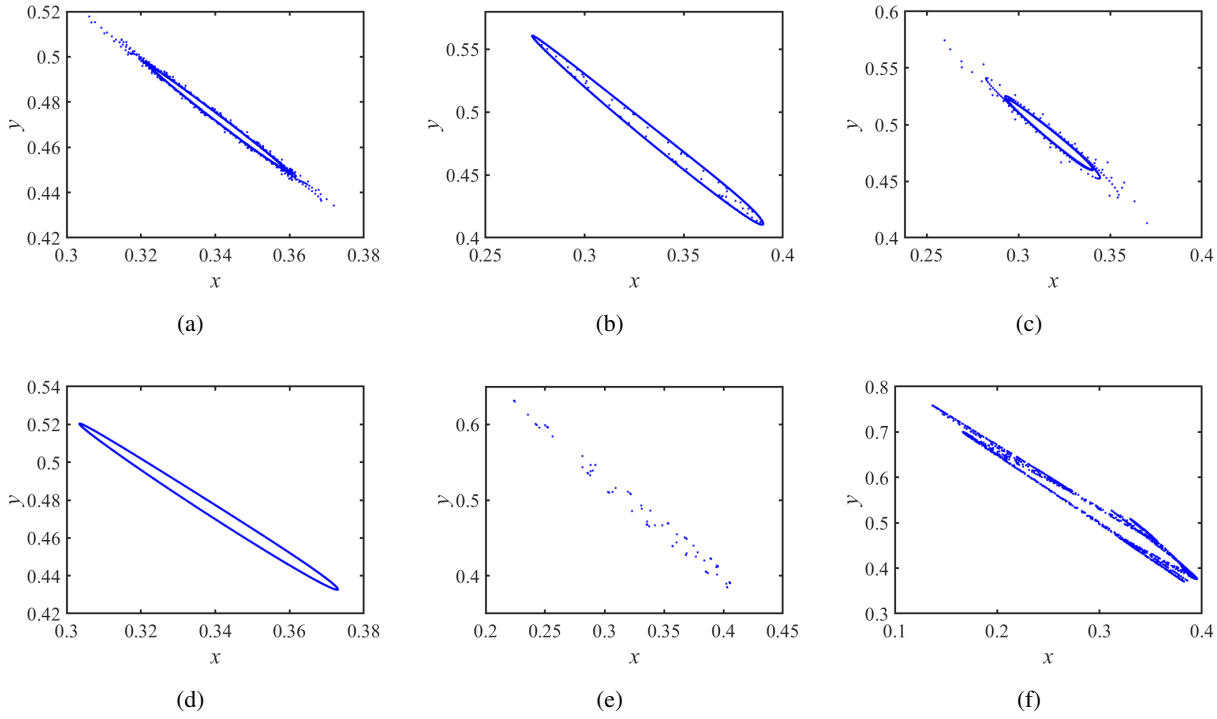

Figure 10. Phase portraits for different values of τ and r. (a) Phase portrait for $\tau = 4.100684389917548$, $r = 1.58$. (b) Phase portrait for $\tau = 4.150684389917548$, $r = 1.58$. (c) A Neimark-Sacker bifurcation occurs when an invariant curve is bifurcated at $\tau = 4.100684389917548$, $r = 1.551$. (d) Stable closed invariant curve for $\tau = 4.114184389917548$ and $r = 1.58$. (e) Period-80 orbit for $\tau = 4.240684389917548$ and $r = 1.58$. (f) Chaos for $\tau = 4.314884389917548$ and $r = 1.551$.

4.4.2. Numerical simulation of 1:3 resonance

Fix parameters $\alpha = 0.032$, $\gamma = 0.149$. The critical parameter values ${\tau_3}^* = 1.684450$, ${r_3}^* = 7.197$ are obtained and model (1.3) has a positive equilibrium point $E^*(x^*, y^*) = (0.257639, 0.110482)$. Further calculations result in

$$\lambda_{41,42} = -0.5000002 \pm 0.867559i,\ \rho_1(0) = 183.642625 + 29.491330i,$$
$$\rho_2(0) = -34.550939 + 20.17372i,\ \mathrm{Re}(\rho_2) = -34.550939 \neq 0.$$

From Theorem 4.2 we can conclude that system (1.3) will undergo a 1:3 strong resonance bifurcation around $E^*(x^*, y^*)$.

Figure 11 illustrates a three-dimensional bifurcation diagram in the (τ, r, x) plane around $E^*(x^*, y^*)$ while parameters τ and r fluctuate within a small region around $({\tau_3}^*, {r_3}^*) = (1.684450, 7.197)$.

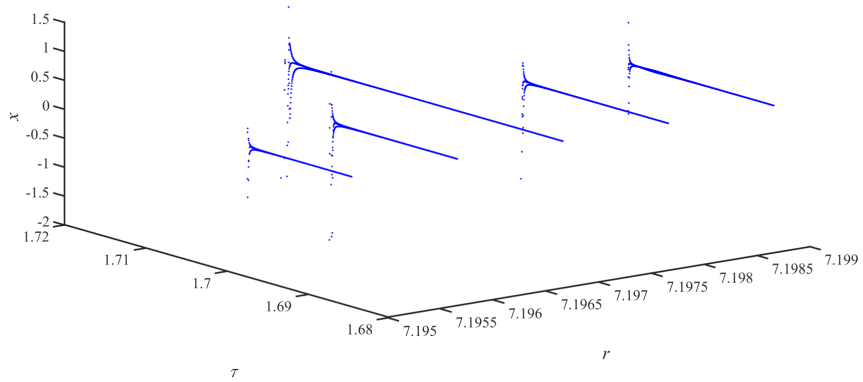

Figure 11. The three-dimensional bifurcation diagram in the (τ, r, x)-space shows the variations when the variables τ and r varied. The parameter r takes on the values 7.195, 7.196, 7.197, 7.198, 7.199 from left to right.

Figure 12(a) depicts a two-dimensional bifurcation diagram in (τ, x) plane when $r = r_3{}^* = 7.197$ and τ fluctuates within the range [1.68, 1.72]. Figure 12(b) displays the maximum Lyapunov exponents associated with Figure 12(a). It reveals the existence of stable fixed points or stable periodic windows within the chaotic region. In this region, some of the maximum Lyapunov exponents are positive while others are negative.

Figure 13(a)–(h) displays the phase portraits of model (1.3) around the equilibrium point $E^*(x^*, y^*)$ with different parameters τ and r close to 1:3 resonance point. When taking the parameters $\tau = 1.66445$, $r = 7.185$, it is clear that there exists a fixed point that joins three saddles. Figure 13(g) illustrates a non-degenerate Neimark-Sacker bifurcation appearing at the trivial fixed point. This results in the occurrence of a closed invariant curve at $\tau = 1.6816$ and $r = 7.1848$. Besides, in a certain parameter range, that is, $\tau = 1.68125$, $r = 7.18$, a homoclinic curve is produced by the intersection of the stable and unstable invariant manifolds of the period-three cycle, which is shown in Figure 13(h).

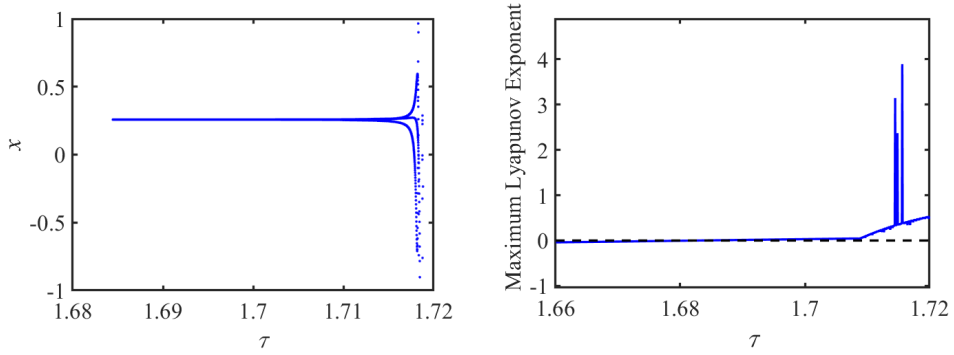

(a) (b)

Figure 12. (a) The bifurcation diagram when a 1:2 strong resonance occurs in (τ, x)-space with $r = 7.197$ and $\tau \in [1.68, 1.72]$. (b) The Maximum Lyapunov exponents associated with (a).

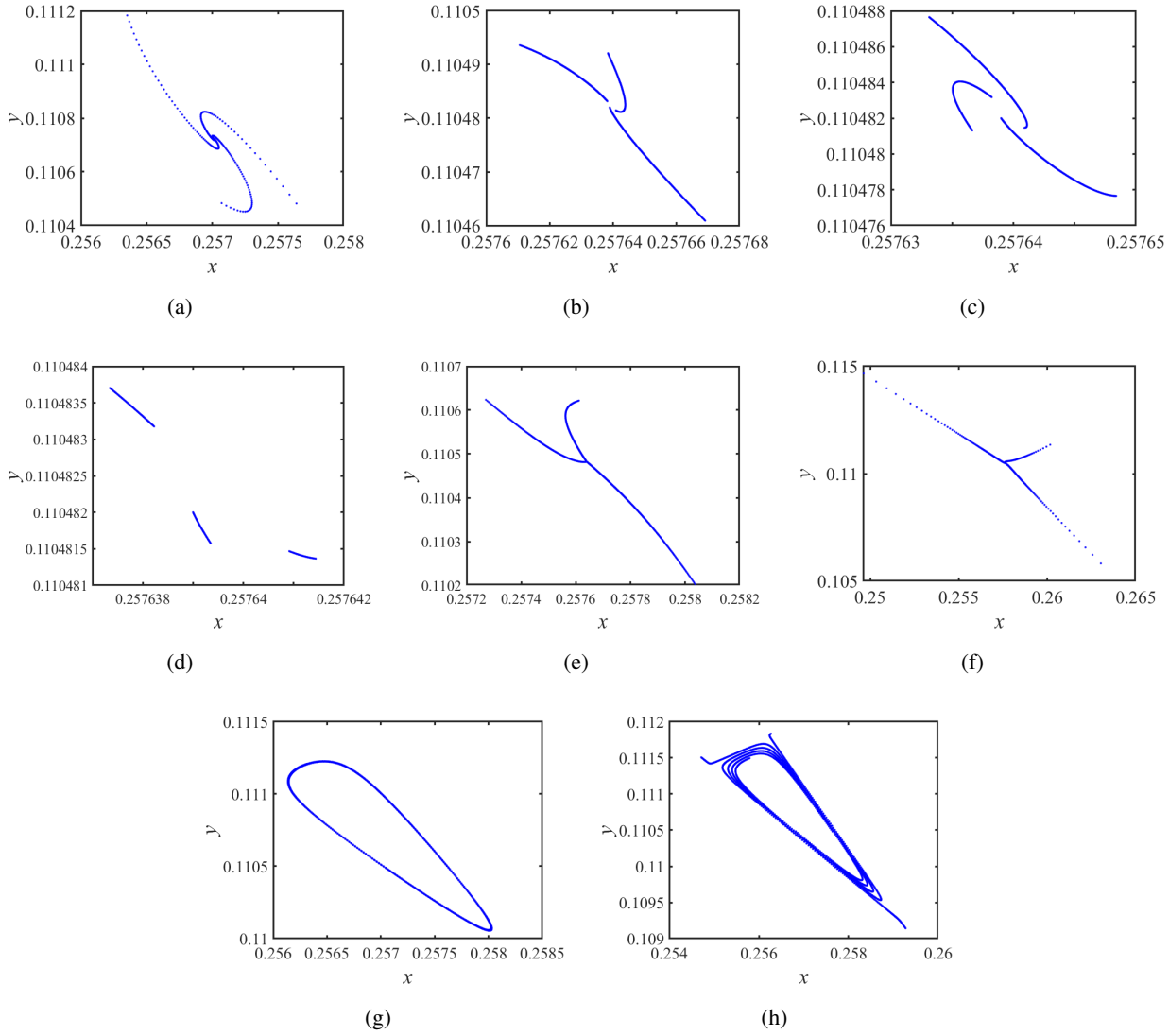

Figure 13. Phase portraits for different values of τ and r near 1:3 resonance point. (a) An attracting 3-point cycle for $\tau = 1.66445,\ r = 7.185$. (b) Phase portrait for $\tau = 1.68465, r = 7.197$. (c) Phase portrait for $\tau = 1.68395,\ r = 7.197$. (d) Phase portrait for $\tau = 1.68445,\ r = 7.197$. (e) Phase portrait for $\tau = 1.68625,\ r = 7.197$. (f) Phase portrait for $\tau = 1.68665,\ r = 7.197$. (g) A closed invariant curve for $\tau = 1.6816,\ r = 7.1848$. (h) Homoclinic structure for $\tau = 1.68125,\ r = 7.18$.

4.4.3. Numerical simulation of 1:4 resonance

Fix parameters $\alpha = 0.0770,\ \gamma = 1.053$. The critical parameter values ${\tau_4}^* = 3.027134312247753$, ${r_4}^* = 6.614$ are obtained and model (1.3) has a positive equilibrium point $E^*(x^*, y^*) = (0.880902017843097, 0.080384004382182)$. Further calculations result in $\lambda_{51,52} = \pm i$, $\mu_1({\tau_4}^*, {r_4}^*) = -74.0446 + 24.0792\text{i}$, $\mu_2({\tau_4}^*, {r_4}^*) = -9.2797 - 12.8233\text{i}$ and $\mu_3({\tau_4}^*, {r_4}^*) = -4.677849 + 1.52123i$. Obviously, in this situation $\text{Re}(\mu_3) = -4.677849 \neq 0$, and $\text{Im}(\mu_3) = 1.52123 \neq 0$. From Theorem 4.3 we can conclude that system (1.3) will undergo a 1:4 strong resonance bifurcation around $E^*(x^*, y^*)$.

Figure 14 illustrates a three-dimensional bifurcation diagram in the (τ, r, x) plane around $E^*(x^*, y^*)$ while parameters τ and r fluctuate within a small region around $(\tau_4{}^*, r_4{}^*) = (3.027134312247753, 6.614)$. Figure 15(a) depicts a two-dimensional bifurcation diagram in (τ, x) plane when $r = r_4{}^* = 6.614$ and τ fluctuates within the range $[2.97, 3.43]$. Figure 15(b) displays the maximum Lyapunov exponents associated with Figure 15(a). It reveals the existence of stable fixed points or stable periodic windows within the chaotic region. In this region, some of the maximum Lyapunov exponents are positive while others are negative.

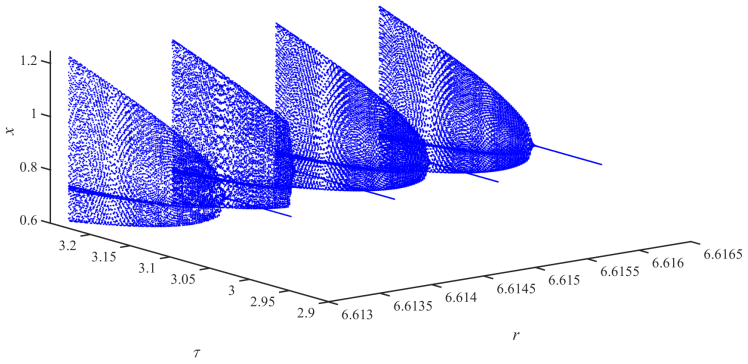

Figure 14. The three-dimensional bifurcation diagram in the (τ, r, x)-space shows the variations when the variables τ and r varied. The parameter r takes on the values $6.613, 6.614, 6.615, 6.616$ from left to right.

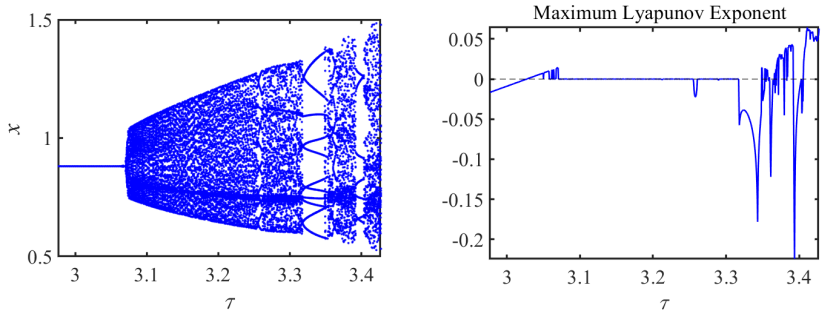

(a) (b)

Figure 15. (a) The bifurcation diagram when a 1:4 strong resonance occurs in (τ, x)-space with $r = 6.614$ and $\tau \in [2.97, 3.43]$. (b) The Maximum Lyapunov exponents associated with (a).

Figure 16(a)–(j) depicts the phase portraits of model (1.3) around the equilibrium point $E^*(x^*, y^*)$ with different parameters τ and r close to 1:4 resonance point. When taking parameters $\tau = 3.027134312247753$ and $r = 6.62$, there is a stable fixed point. Figure 16(e) exhibits a non-degenerate Neimark-Sacker bifurcation appearing at the stable fixed point. This results in the emergence of a closed invariant curve at $\tau = 3.022334312247753$ and $r = 6.61$. According to Figure 16(f)–(i), there are four invariant circles bifurcating from a period-4 orbit as r increases from 6.614 to 6.615, and some cascades of period-doubling bifurcations lead to chaos. These phase portraits demonstrate that

the dynamical behavior of system (1.3) is strongly sensitive to the values of the parameters due to 1:4 resonance.

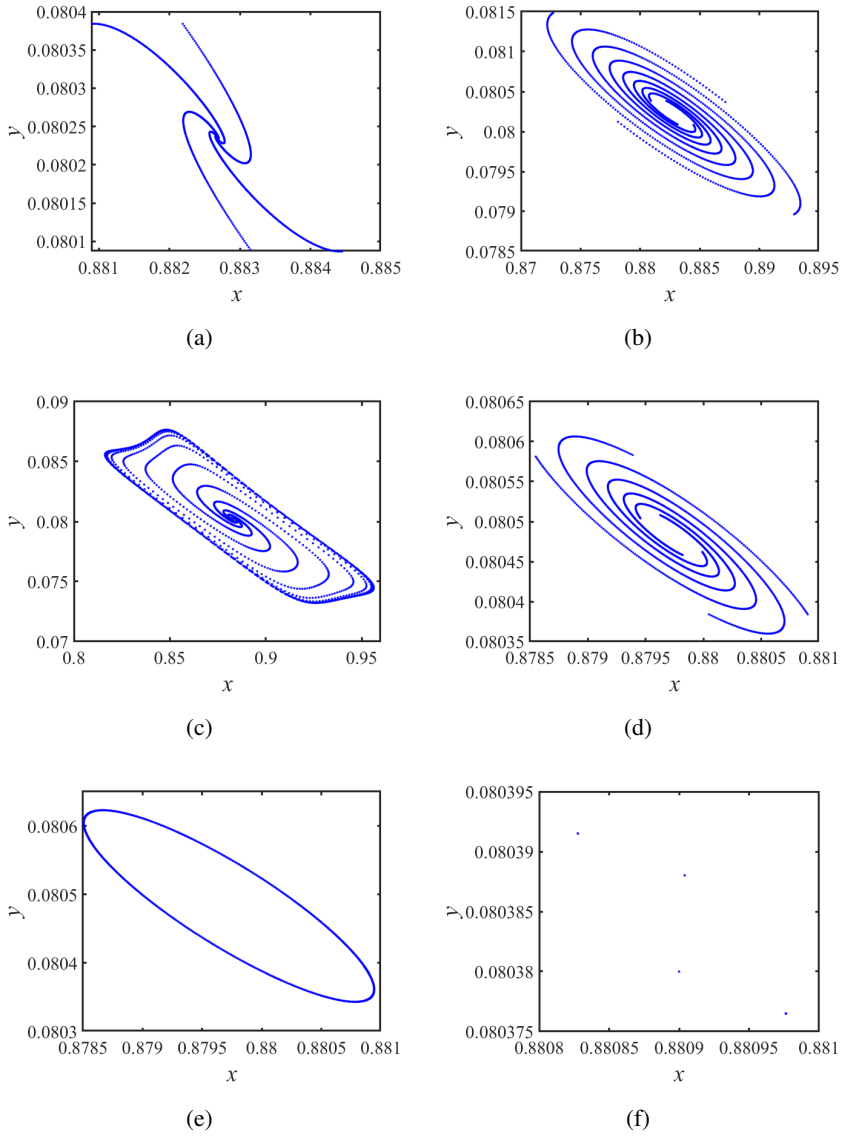

Figure 16. Phase portraits for different values of τ and r near 1:4 resonance point. (a) A stable fixed point for $\tau = 3.027134312247753$, $r = 6.62$. (b) Phase portrait for $\tau = 3.037134312247753$, $r = 6.62$. (c) Phase portrait for $\tau = 3.047134312247753$, $r = 6.62$. (d) Phase portrait for $\tau = 3.020134312247753$, $r = 6.61$. (e) An attracting invariant cycle for $\tau = 3.022334312247753, r = 6.61$. (f) Phase portrait of period-four orbit for $\tau = 3.027134312247753$, $r = 6.614$. (g) Phase portrait for $\tau = 3.017134312247753$, $r = 6.62$. (h) Phase portrait for $\tau = 3.026134312247753$, $r = 6.615$. (i) chaotic attractor for $\tau = 3.427134312247753$, $r = 6.614$. (j) Phase portrait for $\tau = 3.074134312247753$, $r = 6.659$.

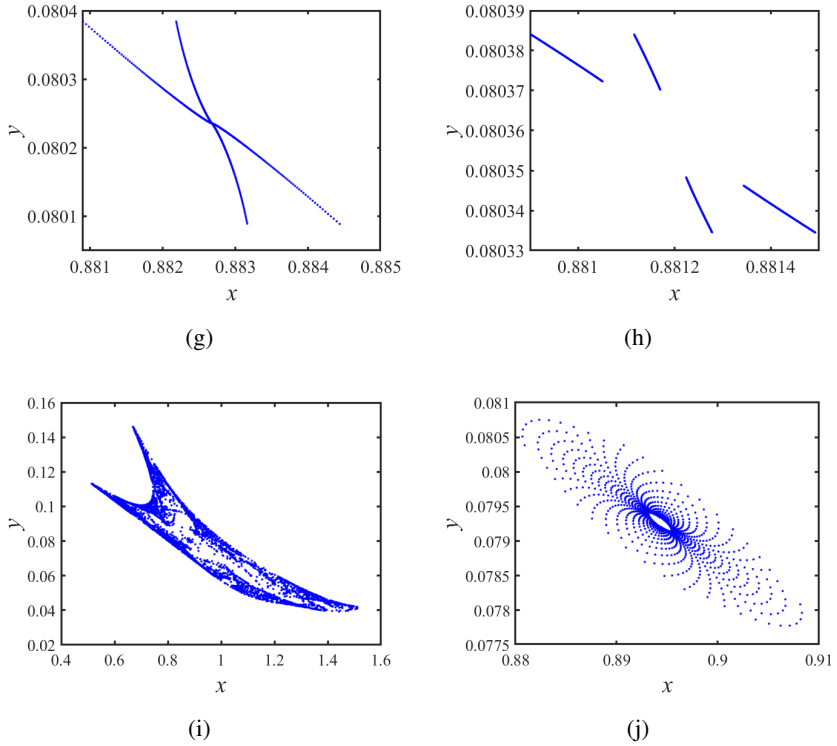

Figure 16. Continued.

5. Conclusions

We studied the complex dynamics of a discrete mussel-algae model without diffusion and advection. It can be seen as the interaction of small-scale mussels with algae in a relatively gentle water. We primarily investigated bifurcations of codimension-one and codimension-two, considering the integral step size as well as other model parameters. The major conclusions are summarized in Theorems 3.1–4.3. Our numerical simulations, including bifurcation diagrams and phase portraits, demonstrate the complicated interactions between mussel and algae.

In this paper, we first considered two kinds of codimension-one bifurcations, including Flip bifurcation and Neimark-Sacker bifurcation. We prove that if Flip bifurcation and Neimark-Sacker bifurcation occurs at $E^*(x^*, y^*)$, and the bifurcation parameter space U and $N.S$ must be satisfied. We provide numerical simulations to verify our theoretical discussions. We can see there exists a 2-periodic stable orbit from the positive point. Similarly, an attracting closed invariant curve bifurcates from the positive equilibrium in Neimark-Sacker circumstances. By numerical simulations, it can be found that both Flip bifurcation and Neimark-Sacker bifurcation will produce chaos. Next, we considered three types of codimension-two bifurcations containing 1:2, 1:3 and 1:4 strong resonance. The system (1.3) can undergo non-degenerate Neimark-Sacker bifurcation, muti-period orbits, and chaotic behaviors due to these strong resonance bifurcations. Our theoretical results reveal that different parameters can lead to complicated dynamical behaviors that can be seen.

Regarding the choice of bifurcation parameters in this study, we provide the following clarifications. While bifurcation results obtained using alternative parameters (e.g., growth rates or mortality rates)

exhibit similarities to those derived with τ as the bifurcation parameter, we primarily selected τ for systematic bifurcation analysis and numerical simulations for the following reasons: By choosing the time step τ as the bifurcation parameter, we aimed to retain the computational simplicity of the dimensionless framework while interpreting τ as a discrete timescale driven by natural or anthropogenic factors. Specifically, τ can be viewed as an implicit temporal scale for artificial interventions. In real-world ecological management (e.g., mussel harvesting or algae regulation), actions are often implemented at fixed intervals (e.g., quarterly), and τ in the model abstracts such management cycles. For instance, an increase in τ may correspond to delayed interventions, prolonging the recovery period of algae after overgrazing by mussels, thereby triggering bifurcations and other dynamic behaviors. Additionally, the mussel-algae interaction inherently exhibits discrete characteristics, such as seasonal mussel reproduction and pulsed algal growth (e.g., the mismatch between mussel feeding cycles and algal growth rates under seasonal variations). Variations in τ reflect adjustments to these natural cycles; for example, climate change-induced elongation of algal growth periods could be simulated by increasing parameter τ.

Concerning the maximum Lyapunov exponent (MLE) plots, slight deviations near certain bifurcation points may arise due to two major factors: (1) The high sensitivity of dynamics near codimension-two bifurcations (e.g., 1:2 and 1:4 resonances), where minor parameter fluctuations may induce transient chaos, and (2) the step-size dependency inherent to finite-difference approximations of Jacobian matrices in numerical computations (despite removing transients). We emphasize that the positive trend in MLE values primarily serves to identify parameter regions where chaos emerges than precisely pinpointing abrupt dynamical shifts at bifurcation points.

In the mussel-algae ecosystem, we identified that the Flip bifurcation causes two species to transition from a steady state gradually through cycles of 2, 4, 8, and multiple cycles, leading to chaos. The Neimark-Sacker bifurcation induces a gradual shift from initial stability to periodic alternating fluctuations in the populations of both species. Several strong resonance bifurcations further characterize the interaction between mussels and algae. The presence of these strong resonance bifurcations indicates that the system's response to periodic perturbations is significantly amplified, causing dynamic behavior to mutate from simple periodic states (e.g., stable equilibrium or 2-period oscillations) to higher-order periods or chaotic states. As bifurcation parameters continue to change, the sequence of period multiplication unfolds, resulting in a chaotic state, which manifests as non-periodic and unpredictable drastic fluctuations in the populations of mussels and algae. Biologically, this process reveals the potential critical response mechanism of the mussel-algae ecosystem to bifurcation parameters: When parameters exceed a threshold, the originally stable balance between mussels and algae may rapidly collapse, causing population dynamics to shift from order to chaos and potentially destabilizing or even collapsing ecological functions. For instance, alternating oscillations can trigger algal blooms and mussel population crashes, leading to chaotic fluctuations that are difficult to predict. The chaotic phenomenon implies unpredictability in population numbers and outbreaks, which hinder monitoring the developmental changes of the two species and maintaining their healthy coexistence. In the ecological management and monitoring of the mussel-algae system, it is crucial to control key parameters such as predation conversion rates and mussel mortality rates within a reasonable bifurcation parameter threshold to prevent parameters from entering the chaotic sensitive region, thereby ensuring the controllability of population dynamics and the resilience of the ecosystem.

In subsequent analyses, building upon the discrete mussel-algae model developed in this study, we

will investigate the effects of spatial diffusion and tidal/wave-induced advection on the two-population system to further enrich the dynamics of the two species.

Author contributions

Qingkai Xu: Conceptualization, Formal analysis, Writing–review & editing; Chunrui Zhang: Methodology, Writing–review; Xingjian Wang: Review, Conceptualization, Resources. All authors have read and approved the final version of the manuscript for publication.

Use of Generative-AI tools declaration

The authors declare they have not used Artificial Intelligence (AI) tools in the creation of this article.

Acknowledgments

This work was supported by the Natural Science Foundation of Heilongjiang Province, under grant No. (LH2020C048). Therefore, the authors thank the Natural Science Foundation of Heilongjiang Province for its financial support.

Conflict of interest

The authors declare that there is no conflicts of interest.

References

1. W. J. Qin, X. W. Tan, X. T. Shi, J. H. Chen, X. Z. Liu, Dynamics and bifurcation analysis of a Filippov predator-prey ecosystem in a seasonally fluctuating environment, *Int. J. Bifur. Chaos*, **29** (2019), 1950020. https://doi.org/10.1142/S0218127419500202
2. X. X. Li, H. G. Yu, C. J. Dai, Z. L. Ma, Q. Wang, M. Zhao, Bifurcation analysis of a new aquatic ecological model with aggregation effect, *Math. Comput. Simul.*, **190** (2021), 75–96. https://doi.org/10.1016/j.matcom.2021.05.015
3. G. A. K. van Voorn, B. W. Kooi, Combining bifurcation and sensitivity analysis for ecological models, *Eur. Phys. J. Spec. Top.*, **226** (2017), 2101–2118. https://doi.org/10.1140/epjst/e2017-70030-2
4. Y. L. Song, H. P. Jiang, Q. X. Liu, Y. Yuan, Spatiotemporal dynamics of the diffusive mussel-algae model near Turing-Hopf bifurcation, *SIAM J. Appl. Dyn. Syst.*, **16** (2017), 2030–2062. https://doi.org/10.1137/16M1097560
5. S. Djilali, B. Ghanbari, S. Bentout, A. Mezouaghi, Turing-Hopf bifurcation in a diffusive mussel-algae model with time-fractional-order derivative, *Chaos Solitons Fract.*, **138** (2020), 109954. https://doi.org/10.1016/j.chaos.2020.109954
6. Z. C. Jiang, W. C. Zhang, Bifurcation analysis in a diffusion mussel-algae interaction system with delays considering the half-saturation constant, *Nonlinear Dyn.*, **108** (2022), 2793–2814. https://doi.org/10.1007/s11071-022-07316-7

7. S. H. Zhong, J. D. Xia, B. Liu, Spatiotemporal dynamics analysis of a semi-discrete reaction-diffusion mussel-algae system with advection, *Chaos Solitons Fract.*, **151** (2021), 111282. https://doi.org/10.1016/j.chaos.2021.111282
8. J. van de Koppel, M. Rietkerk, N. Dankers, P. M. J. Herman, Scale-dependent feedback and regular spatial patterns in young mussel beds, *Am. Nat.*, **165** (2005), E66–E77. https://doi.org/10.1086/428362
9. A. J. Koch, H. Meinhardt, Biological pattern formation: from basic mechanisms to complex structures, *Rev. Mod. Phys.*, **66** (1994), 1481. https://doi.org/10.1103/RevModPhys.66.1481
10. J. A. Sherratt, Periodic traveling waves in integrodifferential equations for nonlocal dispersal, *SIAM J. Appl. Dyn. Syst.*, **13** (2014), 1517–1541. https://doi.org/10.1137/140969725
11. S. Kondo, T. Miura, Reaction-diffusion model as a framework for understanding biological pattern formation, *Science*, **329** (2010), 1616–1620. https://doi.org/10.1126/science.1179047
12. N. Ahmed, A. Elsonbaty, A. Raza, M. Rafiq, W. Adel, Numerical simulation and stability analysis of a novel reaction-diffusion COVID-19 model, *Nonlinear Dyn.*, **106** (2021), 1293–1310. https://doi.org/10.1007/s11071-021-06623-9
13. Y. Lou, R. B. Salako, Mathematical analysis of the dynamics of some reaction-diffusion models for infectious diseases, *J. Differ. Equ.*, **370** (2023), 424–469. https://doi.org/10.1016/j.jde.2023.06.018
14. J. van de Koppel, J. C. Gascoigne, G. Theraulaz, M. Rietkerk, W. M. Mooij, P. M. J. Herman, Experimental evidence for spatial self-organization and its emergent effects in mussel bed ecosystems, *Science*, **322** (2008), 739–742. https://doi.org/10.1126/science.1163952
15. Q. X. Liu, E. J. Weerman, P. M. J. Herman, H. Olff, J. van de Koppel, Alternative mechanisms alter the emergent properties of self-organization in mussel beds, *Proc. R. Soc. B*, **279** (2012), 2744–2753. https://doi.org/10.1098/rspb.2012.0157
16. Q. X. Liu, A. Doelman, V. Rottschafer, M. de Jager, P. M. J. Herman, M. Rietkerk, et al., Phase separation explains a new class of self-organized spatial patterns in ecological systems, *Proc. Natl. Acad. Sci. U.S.A.*, **110** (2013), 11905–11910. https://doi.org/10.1073/pnas.1222339110
17. R. H. Wang, Q. X. Liu, G. Q. Sun, Z. Jin, J. van de Koppel, Nonlinear dynamic and pattern bifurcations in a model for spatial patterns in young mussel beds, *J. R. Soc. Interface*, **6** (2009), 705–718. https://doi.org/10.1098/rsif.2008.0439
18. R. A. Cangelosi, D. J. Wollkind, B. J. Kealy-Dichone, I. Chaiya, Nonlinear stability analyses of Turing patterns for a mussel-algae model, *J. Math. Biol.*, **70** (2015), 1249–1294. https://doi.org/10.1007/s00285-014-0794-7
19. H. P. Jiang, Delay-included Turing-Hopf bifurcation in the diffusive mussel-algae model, *Math. Methods Appl. Sci.*, **44** (2021), 8638–8647. https://doi.org/10.1002/mma.7290
20. N. Chafee, Asymptotic behavior for solutions of a one-dimensional parabolic equation with homogeneous Neumann boundary conditions, *J. Differ. Equ.*, **18** (1975), 111–134. https://doi.org/10.1016/0022-0396(75)90084-4
21. T. Faria, L. T. Magalhaes, Normal forms for retarded functional differential equations with parameters and applications to Hopf bifurcation, *J. Differ. Equ.*, **122** (1995), 181–200. https://doi.org/10.1006/jdeq.1995.1144

22. J. Guckenheimer, Bifurcations of dynamical systems, In: *Dynamical systems*, Boston, MA: Birkhäuser, 1980, 5–123. https://doi.org/10.1007/978-1-4899-3743-8_1

23. Y. A. Kuznetsov, I. A. Kuznetsov, Y. Kuznetsov, *Elements of applied bifurcation theory*, New York: Springer, 1998.

24. M. B. D'Amico, G. R. Chen, E. E. Paolini, J. L. Moiola, Controlling Neimark-Sacker bifurcations in discrete-time multivariable systems, *Syst. Control Lett.*, **58** (2009), 359–364. https://doi.org/10.1016/j.sysconle.2009.01.002

25. L. Li, Z. Wang, Y. X. Li, H. Shen, J. W. Lu, Hopf bifurcation analysis of a complex-valued neural network model with discrete and distributed delays, *Appl. Math. Comput.*, **330** (2018), 152–169. https://doi.org/10.1016/j.amc.2018.02.029

26. D. P. Hu, H. J. Cao, Bifurcation and chaos in a discrete-time predator-prey system of Holling and Leslie type, *Commun. Nonlinear Sci. Numer. Simul.*, **22** (2015), 702–715. https://doi.org/10.1016/j.cnsns.2014.09.010

27. Z. Eskandari, J. Alidousti, Stability and codimension 2 bifurcations of a discrete time SIR model, *J. Franklin Inst.*, **357** (2020), 10937–10959. https://doi.org/10.1016/j.jfranklin.2020.08.040

28. T. S. Parker, L. Chua, *Practical numerical algorithms for chaotic systems*, Springer Science & Business Media, 2012.

29. M. G. Crandall, P. H. Rabinowitz, The Hopf bifurcation theorem in infinite dimensions, *Arch. Ration. Mech. Anal.*, **67** (1977), 53–72. https://doi.org/10.1007/BF00280827

30. V. A. Kim, R. I. Parovik, Application of the explicit Euler method for numerical analysis of a nonlinear fractional oscillation equation, *Fractal Fract.*, **6** (2022), 1–19. https://doi.org/10.3390/fractalfract6050274

31. L. M. Zhang, Y. K. Xu, G. Y. Liao, Codimension-two bifurcations and bifurcation controls in a discrete biological system with weak Allee effect, *Int. J. Bifur. Chaos*, **32** (2022), 2250036. https://doi.org/10.1142/S0218127422500365

32. J. Y. Ma, M. X. Duan, Codimension-two bifurcations of a two-dimensional discrete time Lotka-Volterra predator-prey model, *Discrete Contin. Dyn. Syst. B*, **29** (2024), 1217–1242. https://doi.org/10.3934/dcdsb.2023131

Appendix

The coefficients appearing in several formulas

A. B_{ij}, C_{ij} and D_{ij} in Eq (3.4)

$$B_{11} = \frac{1}{\Omega r\gamma(1+\lambda_{12})} + \frac{\left(-1+\lambda_{12}-\frac{\tau^*[-1+\Omega]}{\Omega^2}\right)}{\Omega^2\tau^* r(1+\lambda_{12})},\ B_{12} = \frac{\Omega r\alpha}{\gamma(1+\lambda_{12})} + \frac{\left(-1+\lambda_{12}-\frac{\tau^*[-1+\Omega]}{\Omega^2}\right)}{\tau^*(1+\lambda_{12})},$$
$$C_{11} = \frac{-1+\lambda_{12}-\frac{\tau^*(\Omega-1)}{\Omega^2}}{\Omega^3 r(\Omega-1)(1+\lambda_{12})},\ C_{12} = \frac{\tau^*}{\gamma(1+\lambda_{12})} + \frac{-1+\lambda_{12}-\frac{\tau^*(\Omega-1)}{\Omega^2}}{(\Omega-1)(1+\lambda_{12})},$$
$$C_{13} = C_{14} = C_{15} = C_{16} = C_{17} = 0,$$

$$D_{11} = \frac{-1+\lambda_{12}-\frac{\tau^*(\Omega-1)}{\Omega^2}}{\Omega^3\tau^* r(\Omega-1)(1+\lambda_{12})},\ D_{12} = \frac{1}{\gamma(1+\lambda_{12})} + \frac{-1+\lambda_{12}-\frac{\tau^*(\Omega-1)}{\Omega^2}}{\tau^*(\Omega-1)(1+\lambda_{12})},\ D_{13} = 0,$$
$$B_{21} = \frac{1}{\Omega r\gamma(1+\lambda_{12})} + \frac{\left(2+\frac{\tau^*[-1+\Omega]}{\Omega^2}\right)}{\Omega^2\tau^* r(1+\lambda_{12})},\ B_{22} = \frac{\Omega r\alpha}{\gamma(1+\lambda_{12})} + \frac{\left(2+\frac{\tau^*[-1+\Omega]}{\Omega^2}\right)}{\tau^*(1+\lambda_{12})},$$
$$C_{21} = \frac{2+\frac{\tau^*(\Omega-1)}{\Omega^2}}{\Omega^3 r(\Omega-1)(1+\lambda_{12})},\ C_{22} = \frac{\tau^*}{\gamma(1+\lambda_{12})} + \frac{2+\frac{\tau^*(\Omega-1)}{\Omega^2}}{(\Omega-1)(1+\lambda_{12})},$$
$$C_{23} = C_{24} = C_{25} = C_{26} = C_{27} = 0,$$
$$D_{21} = \frac{2+\frac{\tau^*(\Omega-1)}{\Omega^2}}{\Omega^3\tau^* r(\Omega-1)(1+\lambda_{12})},\ D_{22} = \frac{1}{\gamma(1+\lambda_{12})} + \frac{2+\frac{\tau^*(\Omega-1)}{\Omega^2}}{\tau^*(\Omega-1)(1+\lambda_{12})},\ D_{23} = 0.$$

B. $m_{ij},\ q_{ij}$ **in Eq (3.5)**

$$\begin{aligned}
m_{11} &= B_{11}T_{11} + B_{12}T_{21}\\
&= \left(\frac{1}{\Omega r\gamma(1+\lambda_{12})} + \frac{-1+\lambda_{12}-\frac{\tau^*[-1+\Omega]}{\Omega^2}}{\Omega^2\tau^* r(1+\lambda_{12})}\right)\cdot(\tau^* r(\Omega-1))\\
&\quad + \left(\frac{\Omega r\alpha}{\gamma(1+\lambda_{12})} + \frac{-1+\lambda_{12}-\frac{\tau^*[-1+\Omega]}{\Omega^2}}{\tau^*(1+\lambda_{12})}\right)\cdot\left(-2-\frac{\tau^*(\Omega-1)}{\Omega^2}\right),\\
m_{12} &= B_{11}T_{12} + B_{12}T_{22}\\
&= \left(\frac{1}{\Omega r\gamma(1+\lambda_{12})} + \frac{-1+\lambda_{12}-\frac{\tau^*[-1+\Omega]}{\Omega^2}}{\Omega^2\tau^* r(1+\lambda_{12})}\right)\cdot(\tau^* r(\Omega-1))\\
&\quad + \left(\frac{\Omega r\alpha}{\gamma(1+\lambda_{12})} + \frac{-1+\lambda_{12}-\frac{\tau^*[-1+\Omega]}{\Omega^2}}{\tau^*(1+\lambda_{12})}\right)\cdot\left(-1+\lambda_{12}-\frac{(-1+\Omega)\tau^*}{\Omega^2}\right),\\
m_{13} &= C_{11}T_{11}^2 + C_{12}T_{11}T_{21} + C_{13}T_{21}^2\\
&= \left(\frac{-1+\lambda_{12}-\frac{\tau^*(\Omega-1)}{\Omega^2}}{\Omega^3 r(\Omega-1)(1+\lambda_{12})}\right)\cdot(\tau^* r(\Omega-1))^2\\
&\quad + \left(\frac{\tau^*}{\gamma(1+\lambda_{12})} + \frac{-1+\lambda_{12}-\frac{\tau^*(\Omega-1)}{\Omega^2}}{(\Omega-1)(1+\lambda_{12})}\right)\cdot(\tau^* r(\Omega-1))\cdot\left(-2-\frac{\tau^*(\Omega-1)}{\Omega^2}\right),\\
m_{14} &= 2C_{11}T_{11}T_{12} + C_{12}T_{12}T_{21} + C_{12}T_{11}T_{22} + 2C_{13}T_{21}T_{22}\\
&= \frac{2r[-1+\Omega](\tau^*)^2\left(-1+\lambda_{12}-\frac{\tau^*[-1+\Omega]}{\Omega^2}\right)}{\Omega^3(1+\lambda_{12})}\\
&\quad + r[-1+\Omega]\tau^*\left(-1+\lambda_{12}-\frac{(-1+\Omega)\tau^*}{\Omega^2}\right)\left(\frac{\tau^*}{\gamma[1+\lambda_{12}]} + \frac{-1+\lambda_{12}-\frac{\tau^*[-1+\Omega]}{\Omega^2}}{(-1+\Omega)(1+\lambda_{12})}\right)\\
&\quad + r[-1+\Omega]\tau^*\left(-2-\frac{\tau^*[-1+\Omega]}{\Omega^2}\right)\left(\frac{\tau^*}{\gamma[1+\lambda_{12}]} + \frac{-1+\lambda_{12}-\frac{\tau^*[-1+\Omega]}{\Omega^2}}{(-1+\Omega)(1+\lambda_{12})}\right),\\
m_{15} &= C_{11}T_{12}^2 + C_{12}T_{12}T_{22} + C_{13}T_{22}^2
\end{aligned}$$

$$= \left(\frac{-1+\lambda_{12}-\frac{\tau^*(\Omega-1)}{\Omega^2}}{\Omega^3 r(\Omega-1)(1+\lambda_{12})}\right)\cdot(\tau^* r(\Omega-1))^2$$
$$+\left(\frac{\tau^*}{\gamma(1+\lambda_{12})}+\frac{-1+\lambda_{12}-\frac{\tau^*(\Omega-1)}{\Omega^2}}{(\Omega-1)(1+\lambda_{12})}\right)\cdot(\tau^* r(\Omega-1))\cdot\left(-1+\lambda_{12}-\frac{(-1+\Omega)\tau^*}{\Omega^2}\right),$$

$$m_{16} = C_{14}T_{11}^3 + C_{15}T_{11}^2T_{21} + C_{16}T_{11}T_{21}^2 + C_{17}T_{21}^3 = 0,$$

$$m_{17} = 3C_{14}T_{11}^2T_{12} + 2C_{15}T_{11}T_{12}T_{21} + C_{16}T_{12}T_{21}^2 + C_{15}T_{11}^2T_{22} + 2C_{16}T_{11}T_{21}T_{22} + 3C_{17}T_{21}^2T_{22} = 0,$$

$$m_{18} = 3C_{14}T_{11}T_{12}^2 + 2C_{15}T_{11}T_{12}T_{22} + C_{16}T_{11}T_{22}^2 + C_{15}T_{12}^2T_{21} + 2C_{16}T_{12}T_{21}T_{22} + 3C_{17}T_{21}T_{22}^2 = 0,$$

$$m_{19} = C_{14}T_{12}^3 + C_{15}T_{12}^2T_{22} + C_{16}T_{12}T_{22}^2 + C_{17}T_{22}^3 = 0,$$

$$q_{11} = D_{11}T_{11}^2 + D_{12}T_{11}T_{21} + D_{13}T_{21}^2$$
$$= \frac{(-1+\Omega)r\tau^*\left(-1+\lambda_{12}-\frac{\tau^*[-1+\Omega]}{\Omega^2}\right)}{\Omega^3(1+\lambda_{12})}$$
$$+(-1+\Omega)r\tau^*\left(-2-\frac{(-1+\Omega)\tau^*}{\Omega^2}\right)\left(\frac{1}{\gamma[1+\lambda_{12}]}+\frac{-1+\lambda_{12}-\frac{\tau^*[-1+\Omega]}{\Omega^2}}{(-1+\Omega)(1+\lambda_{12})\tau^*}\right),$$

$$q_{12} = D_{11}T_{12}^2 + D_{12}T_{12}T_{22} + D_{13}T_{22}^2$$
$$= \frac{(-1+\Omega)r\tau^*\left(-1+\lambda_{12}-\frac{\tau^*[-1+\Omega]}{\Omega^2}\right)}{\Omega^3(1+\lambda_{12})}$$
$$+(-1+\Omega)r\tau^*\left(-1+\lambda_{12}-\frac{(-1+\Omega)\tau^*}{\Omega^2}\right)\left(\frac{1}{\gamma[1+\lambda_{12}]}+\frac{-1+\lambda_{12}-\frac{\tau^*[-1+\Omega]}{\Omega^2}}{(-1+\Omega)(1+\lambda_{12})\tau^*}\right),$$

$$q_{13} = 2D_{11}T_{11}T_{12} + D_{12}T_{12}T_{21} + D_{12}T_{11}T_{22} + 2D_{13}T_{21}T_{22}$$
$$= \frac{2(-1+\Omega)r\tau^*\left(-1+\lambda_{12}-\frac{\tau^*[-1+\Omega]}{\Omega^2}\right)}{\Omega^3(1+\lambda_{12})}$$
$$+(-1+\Omega)r\tau^*\left(-2-\frac{(-1+\Omega)\tau^*}{\Omega^2}\right)\left(\frac{1}{\gamma[1+\lambda_{12}]}+\frac{-1+\lambda_{12}-\frac{\tau^*[-1+\Omega]}{\Omega^2}}{(-1+\Omega)(1+\lambda_{12})\tau^*}\right)$$
$$+(-1+\Omega)r\tau^*\left(-1+\lambda_{12}-\frac{(-1+\Omega)\tau^*}{\Omega^2}\right)\left(\frac{1}{\gamma[1+\lambda_{12}]}+\frac{-1+\lambda_{12}-\frac{\tau^*[-1+\Omega]}{\Omega^2}}{(-1+\Omega)(1+\lambda_{12})\tau^*}\right),$$

$$m_{21} = B_{21}T_{11} + B_{22}T_{21}$$
$$= \left(\frac{1}{\Omega r\gamma(1+\lambda_{12})}+\frac{2+\frac{\tau^*[-1+\Omega]}{\Omega^2}}{\Omega^2\tau^* r(1+\lambda_{12})}\right)\cdot(\tau^* r(\Omega-1))$$
$$+\left(\frac{\Omega r\alpha}{\gamma(1+\lambda_{12})}+\frac{2+\frac{\tau^*[-1+\Omega]}{\Omega^2}}{\tau^*(1+\lambda_{12})}\right)\cdot\left(-2-\frac{\tau^*(\Omega-1)}{\Omega^2}\right),$$

$$m_{22} = B_{21}T_{12} + B_{22}T_{22}$$
$$= \left(\frac{1}{\Omega r\gamma(1+\lambda_{12})}+\frac{2+\frac{\tau^*[-1+\Omega]}{\Omega^2}}{\Omega^2\tau^* r(1+\lambda_{12})}\right)\cdot(\tau^* r(\Omega-1))$$

$$+\left(\frac{\Omega r\alpha}{\gamma(1+\lambda_{12})}+\frac{2+\frac{\tau^*[-1+\Omega]}{\Omega^2}}{\tau^*(1+\lambda_{12})}\right)\cdot\left(-1+\lambda_{12}-\frac{(-1+\Omega)\tau^*}{\Omega^2}\right),$$

$$\begin{aligned}
m_{23} &= C_{21}T_{11}^2+C_{22}T_{11}T_{21}+C_{23}T_{21}^2\\
&=\left(\frac{2+\frac{\tau^*(\Omega-1)}{\Omega^2}}{\Omega^3 r(\Omega-1)(1+\lambda_{12})}\right)\cdot(\tau^* r(\Omega-1))^2\\
&\quad+\left(\frac{\tau^*}{\gamma(1+\lambda_{12})}+\frac{2+\frac{\tau^*(\Omega-1)}{\Omega^2}}{(\Omega-1)(1+\lambda_{12})}\right)\cdot(\tau^* r(\Omega-1))\cdot\left(-2-\frac{\tau^*(\Omega-1)}{\Omega^2}\right),\\
m_{24} &= 2C_{21}T_{11}T_{12}+C_{22}T_{12}T_{21}+C_{22}T_{11}T_{22}+2C_{23}T_{21}T_{22}\\
&=\frac{2r[-1+\Omega](\tau^*)^2\left(2+\frac{\tau^*[-1+\Omega]}{\Omega^2}\right)}{\Omega^3(1+\lambda_{12})}\\
&\quad+r[-1+\Omega]\tau^*\left(-1+\lambda_{12}-\frac{(-1+\Omega)\tau^*}{\Omega^2}\right)\left(\frac{\tau^*}{\gamma[1+\lambda_{12}]}+\frac{2+\frac{\tau^*[-1+\Omega]}{\Omega^2}}{(-1+\Omega)(1+\lambda_{12})}\right)\\
&\quad+r[-1+\Omega]\tau^*\left(-2-\frac{\tau^*[-1+\Omega]}{\Omega^2}\right)\left(\frac{\tau^*}{\gamma[1+\lambda_{12}]}+\frac{2+\frac{\tau^*[-1+\Omega]}{\Omega^2}}{(-1+\Omega)(1+\lambda_{12})}\right),\\
m_{25} &= C_{21}T_{12}^2+C_{22}T_{12}T_{22}+C_{23}T_{22}^2\\
&=\left(\frac{2+\frac{\tau^*(\Omega-1)}{\Omega^2}}{\Omega^3 r(\Omega-1)(1+\lambda_{12})}\right)\cdot(\tau^* r(\Omega-1))^2\\
&\quad+\left(\frac{\tau^*}{\gamma(1+\lambda_{12})}+\frac{2+\frac{\tau^*(\Omega-1)}{\Omega^2}}{(\Omega-1)(1+\lambda_{12})}\right)\cdot(\tau^* r(\Omega-1))\cdot\left(-1+\lambda_{12}-\frac{(-1+\Omega)\tau^*}{\Omega^2}\right),\\
m_{26} &= C_{24}T_{11}^3+C_{25}T_{11}^2T_{21}+C_{26}T_{11}T_{21}^2+C_{27}T_{21}^3=0,\\
m_{27} &= 3C_{24}T_{11}^2T_{12}+2C_{25}T_{11}T_{12}T_{21}+C_{26}T_{12}T_{21}^2+C_{25}T_{11}^2T_{22}+2C_{26}T_{11}T_{21}T_{22}+3C_{27}T_{21}^2T_{22}=0,\\
m_{28} &= 3C_{24}T_{11}T_{12}^2+2C_{25}T_{11}T_{12}T_{22}+C_{26}T_{11}T_{22}^2+C_{25}T_{12}^2T_{21}+2C_{26}T_{12}T_{21}T_{22}+3C_{27}T_{21}T_{22}^2=0,\\
m_{29} &= C_{24}T_{12}^3+C_{25}T_{12}^2T_{22}+C_{26}T_{12}T_{22}^2+C_{27}T_{22}^3=0,\\
q_{21} &= D_{21}T_{11}^2+D_{22}T_{11}T_{21}+D_{23}T_{21}^2\\
&=\frac{(-1+\Omega)r\tau^*\left(2+\frac{\tau^*[-1+\Omega]}{\Omega^2}\right)}{\Omega^3(1+\lambda_{12})}\\
&\quad+(-1+\Omega)r\tau^*\left(-2-\frac{(-1+\Omega)\tau^*}{\Omega^2}\right)\left(\frac{1}{\gamma[1+\lambda_{12}]}+\frac{2+\frac{\tau^*[-1+\Omega]}{\Omega^2}}{(-1+\Omega)(1+\lambda_{12})\tau^*}\right),
\end{aligned}$$

$$\begin{aligned}
q_{22} &= D_{21}T_{12}^2+D_{22}T_{12}T_{22}+D_{23}T_{22}^2\\
&=\frac{(-1+\Omega)r\tau^*\left(2+\frac{\tau^*[-1+\Omega]}{\Omega^2}\right)}{\Omega^3(1+\lambda_{12})}\\
&\quad+(-1+\Omega)r\tau^*\left(-1+\lambda_{12}-\frac{(-1+\Omega)\tau^*}{\Omega^2}\right)\left(\frac{1}{\gamma[1+\lambda_{12}]}+\frac{2+\frac{\tau^*[-1+\Omega]}{\Omega^2}}{(-1+\Omega)(1+\lambda_{12})\tau^*}\right),
\end{aligned}$$

$$
\begin{aligned}
q_{23} &= 2D_{21}T_{11}T_{12} + D_{22}T_{12}T_{21} + D_{22}T_{11}T_{22} + 2D_{23}T_{21}T_{22}\\
&= \frac{2\left(-1+\Omega\right)r\tau^*\left(2+\frac{\tau^*[-1+\Omega]}{\Omega^2}\right)}{\Omega^3\left(1+\lambda_{12}\right)}\\
&\quad + \left(-1+\Omega\right)r\tau^*\left(-2-\frac{\left(-1+\Omega\right)\tau^*}{\Omega^2}\right)\left(\frac{1}{\gamma\left[1+\lambda_{12}\right]}+\frac{2+\frac{\tau^*[-1+\Omega]}{\Omega^2}}{\left(-1+\Omega\right)\left(1+\lambda_{12}\right)\tau^*}\right)\\
&\quad + \left(-1+\Omega\right)r\tau^*\left(-1+\lambda_{12}-\frac{\left(-1+\Omega\right)\tau^*}{\Omega^2}\right)\left(\frac{1}{\gamma\left[1+\lambda_{12}\right]}+\frac{2+\frac{\tau^*[-1+\Omega]}{\Omega^2}}{\left(-1+\Omega\right)\left(1+\lambda_{12}\right)\tau^*}\right).
\end{aligned}
$$

C. $\vartheta_{ij},\ \upsilon_{ij}$ in Eq (4.7)

$$
\begin{aligned}
\vartheta_{20}(\tau,r) &= f_{20}+\psi_{20}-2\varphi_{20}-\tilde{e}_{10}^2\varphi_{02}+\tilde{e}_{10}\varphi_{11},\\
\vartheta_{11}(\tau,r) &= f_{11}+\psi_{11}+2\varphi_{20}-2\tilde{e}_{10}(-1+\tilde{e}_{01})\varphi_{02}-(2+\tilde{e}_{10}-\tilde{e}_{01})\varphi_{11},\\
\vartheta_{02}(\tau,r) &= -\varphi_{20}+\psi_{02}-(-1+\tilde{e}_{01})\varphi_{11}-(2-2\tilde{e}_{01}+\tilde{e}_{01}^2)\varphi_{02},\\
\vartheta_{30}(\tau,r) &= -\varphi_{30}+2f_{20}\varphi_{20}+f_{30}+\psi_{30}+f_{11}\psi_{20}+\alpha_{30}-\tilde{e}_{10}\alpha_{21}+\tilde{e}_{10}^2\alpha_{12}-\tilde{e}_{10}^3\alpha_{03}\\
&\quad -(2\tilde{e}_{10}^2\varphi_{20}+2\tilde{e}_{10}(-1+\tilde{e}_{01})\psi_{20}+2\tilde{e}_{10}g_{20})\varphi_{02}\\
&\quad -(-2\tilde{e}_{10}\varphi_{20}+(1-\tilde{e}_{01}+\tilde{e}_{10})\psi_{20}+\tilde{e}_{10}f_{20}-g_{20})\varphi_{11}\\
&\quad -(2\varphi_{20}-2\psi_{20}-2f_{20})\varphi_{20},\\
\vartheta_{21}(\tau,r) &= -\varphi_{21}+2f_{20}\varphi_{11}+\psi_{21}+f_{11}(\psi_{11}+\varphi_{20})-3\alpha_{30}\\
&\quad -(-1+\tilde{e}_{01}-2\tilde{e}_{10})\alpha_{21}-(\tilde{e}_{10}^2-2\tilde{e}_{10}(-1+\tilde{e}_{01}))\alpha_{12}\\
&\quad -3\tilde{e}_{10}^2(-1+\tilde{e}_{01})\alpha_{03}-\varphi_{02}[2\tilde{e}_{10}^2\varphi_{11}+2\tilde{e}_{10}(-1+\tilde{e}_{01})(\psi_{11}+\varphi_{20})\\
&\quad +2(-1+\tilde{e}_{01})^2\psi_{20}+2g_{20}(-1+\tilde{e}_{01})+2\tilde{e}_{10}g_{11}]\\
&\quad -\varphi_{11}[-2\tilde{e}_{10}\varphi_{11}+(1-\tilde{e}_{01}+\tilde{e}_{10})(\psi_{11}+\varphi_{20})+2(-1+\tilde{e}_{01})\psi_{20}\\
&\quad +f_{20}(-1+\tilde{e}_{01})-g_{11}+g_{20}+\tilde{e}_{10}f_{11}]\\
&\quad -\varphi_{20}[2\varphi_{11}-2(\psi_{11}+\varphi_{20})+2\psi_{20}+2f_{20}-2f_{11}],\\
\vartheta_{12}(\tau,r) &= -\varphi_{12}+\psi_{12}+2\varphi_{20}\psi_{02}-2\tilde{e}_{10}^2\varphi_{02}^2+2(f_{02}-f_{11})\varphi_{20}+2f_{11}\varphi_{11}\\
&\quad -2(\varphi_{02}-\varphi_{11})\varphi_{20}+2f_{02}\psi_{11}+(\tilde{e}_{01}-\tilde{e}_{10}-1)\varphi_{11}\psi_{02}\\
&\quad -2(1-\tilde{e}_{01})^2\varphi_{02}\psi_{11}+2(1-\tilde{e}_{01})\varphi_{11}\psi_{11}-2(g_{02}\tilde{e}_{10}-f_{20}+(\tilde{e}_{01}-1)g_{11})\varphi_{02}\\
&\quad +(\tilde{e}_{01}-\tilde{e}_{10}-1)\varphi_{11}^2+2\alpha_{12}(1-\tilde{e}_{01})\tilde{e}_{10}-(f_{11}\tilde{e}_{01}+f_{02}\tilde{e}_{10}-g_{02}+g_{11})\varphi_{11}\\
&\quad +f_{11}\psi_{02}-2\varphi_{20}\psi_{11}-2(\tilde{e}_{01}-2)\tilde{e}_{10}\varphi_{11}\varphi_{02}+2\tilde{e}_{10}(1-\tilde{e}_{01})\varphi_{02}\psi_{02}\\
&\quad -3\alpha_{03}(1-\tilde{e}_{01})^2\tilde{e}_{10}-2\alpha_{21}(1-\tilde{e}_{01})+\alpha_{12}(1-\tilde{e}_{01})^2-\alpha_{21}\tilde{e}_{10}+3\alpha_{30},\\
\vartheta_{03}(\tau,r) &= 2f_{02}\psi_{02}-2(1-\tilde{e}_{01})^2\varphi_{02}\psi_{02}+2(1-\tilde{e}_{01})\varphi_{11}\psi_{02}-2\varphi_{20}\psi_{02}+\psi_{03}\\
&\quad +2(1-\tilde{e}_{01})\tilde{e}_{10}\varphi_{02}^2+(f_{11}+2(1-\tilde{e}_{01})g_{02})\varphi_{02}+(-1-\tilde{e}_{10}+\tilde{e}_{01})\varphi_{11}\varphi_{02}\\
&\quad +2\varphi_{02}\varphi_{20}-\alpha_{30}-\alpha_{12}(1-\tilde{e}_{01})^2+\alpha_{21}(1-\tilde{e}_{01})+\alpha_{03}(1-\tilde{e}_{01})^3-\varphi_{03}\\
&\quad +(-g_{02}+(1-\tilde{e}_{01})f_{02})\varphi_{11}-2f_{02}\varphi_{20},\\
\upsilon_{20}(\tau,r) &= g_{20}-\psi_{02}\tilde{e}_{10}^2+\tilde{e}_{10}(\psi_{11}+\varphi_{20})+(\tilde{e}_{01}-2)\psi_{20},\\
\upsilon_{11}(\tau,r) &= g_{11}+2\tilde{e}_{10}(1-\tilde{e}_{01})\psi_{02}-(2-2\tilde{e}_{01}+\tilde{e}_{10})\psi_{11}+2\psi_{20}+\varphi_{11}\tilde{e}_{10},\\
\upsilon_{02}(\tau,r) &= g_{02}-(2-(3-\tilde{e}_{01})\tilde{e}_{01})\psi_{02}+(1-\tilde{e}_{01})\psi_{11}-\psi_{20}+\tilde{e}_{01}\varphi_{02},
\end{aligned}
$$

$$
\begin{aligned}
\upsilon_{30}(\tau,r) &= 2\tilde{e}_{10}(1-\tilde{e}_{01})\psi_{20}\psi_{02} - 2\tilde{e}_{10}^2\varphi_{20}\psi_{02} - 2\tilde{e}_{10}g_{20}\psi_{02} - (1+\tilde{e}_{10}-\tilde{e}_{01})\psi_{11}\psi_{20}\\
&\quad + 2\tilde{e}_{10}\varphi_{20}\psi_{11} - (f_{20}\tilde{e}_{10}-g_{20})\psi_{11} + 2\psi_{20}^2 + (g_{11}+2f_{20})\psi_{20} - 2\varphi_{20}\psi_{20}\\
&\quad - (1-\tilde{e}_{01})\psi_{30} + 2g_{20}\varphi_{20} + \tilde{e}_{10}\varphi_{30} - \beta_{03}\tilde{e}_{10}^3 - \beta_{21}\tilde{e}_{10} + \beta_{30} + \beta_{12}\tilde{e}_{10}^2,\\
\upsilon_{21}(\tau,r) &= -\psi_{21}(1-\tilde{e}_{01}) + 2g_{20}\varphi_{11} + \varphi_{21}\tilde{e}_{10} + 2\varphi_{20}\psi_{20}\\
&\quad + 2(1-\tilde{e}_{01})\tilde{e}_{10}\psi_{02}\psi_{11} - 2(1-\tilde{e}_{01})^2\psi_{02}\psi_{20} + 2(1-\tilde{e}_{01})\tilde{e}_{10}\varphi_{20}\psi_{02}\\
&\quad - (1+\tilde{e}_{10}-\tilde{e}_{01})\varphi_{20}\psi_{11} + g_{11}\varphi_{20} - (1+\tilde{e}_{10}-\tilde{e}_{01})\psi_{11}^2 + 2(2-\tilde{e}_{01})\psi_{11}\psi_{20}\\
&\quad + 2\tilde{e}_{10}\varphi_{11}\psi_{11} - 2\varphi_{11}\psi_{20} - 2\psi_{20}^2 - 2\tilde{e}_{10}^2\varphi_{11}\psi_{02}\\
&\quad + ((1-\tilde{e}_{01})f_{20} - g_{20} + 2g_{11} - f_{11}\tilde{e}_{10})\psi_{11}\\
&\quad + 2(g_{02} - f_{20} + f_{11})\psi_{20} - \beta_{12}\tilde{e}_{10}^2 - 2\beta_{12}(1-\tilde{e}_{01})\tilde{e}_{10}\\
&\quad + 2((1-\tilde{e}_{01})g_{20} - \tilde{e}_{10}g_{11})\psi_{02} + 3\beta_{03}(1-\tilde{e}_{01})\tilde{e}_{10}^2 + \beta_{21}(1-\tilde{e}_{01}) + 2\beta_{21}\tilde{e}_{10} - 3\beta_{30},\\
\upsilon_{12}(\tau,r) &= g_{11}\varphi_{11} - (1+\tilde{e}_{10}-\tilde{e}_{01})\varphi_{11}\psi_{11} - (2\tilde{e}_{01}^2 - 5\tilde{e}_{01} + 3 - \tilde{e}_{10})\psi_{02}\psi_{11}\\
&\quad + 2\varphi_{11}\psi_{20} + 2\tilde{e}_{10}(1-\tilde{e}_{01})\varphi_{11}\psi_{02} + \tilde{e}_{10}\varphi_{12} - (1-\tilde{e}_{01})\psi_{12} + 2g_{20}\varphi_{02} - 2\varphi_{02}\psi_{20}\\
&\quad - 2\psi_{11}\psi_{20} + 2(f_{02}-f_{11})\psi_{20} + 2(1-\tilde{e}_{01})\psi_{11}^2 + 2\tilde{e}_{10}\varphi_{02}\psi_{11} + 2\tilde{e}_{10}(1-\tilde{e}_{01})\psi_{02}^2\\
&\quad - 2\tilde{e}_{10}^2\varphi_{02}\psi_{02} - (f_{02}\tilde{e}_{10} - 3g_{02} + g_{11} - f_{11}(1-\tilde{e}_{01}))\psi_{11}\\
&\quad + (2(1-\tilde{e}_{01})g_{11} - 2g_{02}\tilde{e}_{10} + g_{11})\psi_{02} + 2\psi_{02}\psi_{20}\\
&\quad - 3\beta_{03}(1-\tilde{e}_{01})^2\tilde{e}_{10} - 2\beta_{21}(1-\tilde{e}_{01}) + \beta_{12}(1-\tilde{e}_{01})^2 - \beta_{21}\tilde{e}_{10} + 3\beta_{30} + 2\beta_{12}(1-\tilde{e}_{01})\tilde{e}_{10},\\
\upsilon_{03}(\tau,r) &= -2(1-\tilde{e}_{01})^2\psi_{02}^2 + 2(1-\tilde{e}_{01})\psi_{02}\psi_{11} - 2\psi_{02}\psi_{20} + 2\tilde{e}_{10}(1-\tilde{e}_{01})\varphi_{02}\psi_{02}\\
&\quad + 2(2-\tilde{e}_{01})g_{02}\psi_{02} - (1-\tilde{e}_{01})\psi_{03} - (1+\tilde{e}_{10}-\tilde{e}_{01})\varphi_{02}\psi_{11} - 2f_{02}\psi_{20} + 2\varphi_{02}\psi_{20}\\
&\quad - (g_{02} - f_{02}(1-\tilde{e}_{01}))\psi_{11} + \beta_{21}(1-\tilde{e}_{01}) - \beta_{12}(1-\tilde{e}_{01})^2 + g_{11}\varphi_{02} + \tilde{e}_{10}\varphi_{03}\\
&\quad + \beta_{03}(1-\tilde{e}_{01})^3 - \beta_{30}.
\end{aligned}
$$

D. $\tilde{\sigma}_{ij}$ in Eq (4.19)

$$
\begin{aligned}
\tilde{\sigma}_{20} &= g_{20} + \frac{1}{2}\sqrt{3}i\sigma_{20},\ \tilde{\sigma}_{11} = g_{11} - \frac{3-\sqrt{3}i}{2}\sigma_{11},\ \tilde{\sigma}_{02} = g_{02},\\
\tilde{\sigma}_{30} &= \frac{3-\sqrt{3}i}{2}\sigma_{20}g_{20} + \frac{1}{2}\bar{\sigma}_{02}g_{11} + g_{30} + \frac{1-\sqrt{3}i}{2}\sigma_{11}\bar{g}_{02} + \frac{3+\sqrt{3}i}{4}\sigma_{20}^2,\\
\tilde{\sigma}_{21} &= \bar{\sigma}_{02}g_{02} + \frac{5+\sqrt{3}i}{2}\sigma_{11}g_{20} + \bar{\sigma}_{11}g_{11} + \frac{2-\sqrt{3}i}{2}\sigma_{20}g_{11} + g_{21}\\
&\quad + \frac{\sqrt{3}i}{2}\sigma_{11}\sigma_{20} + \frac{1-\sqrt{3}i}{2}\sigma_{11}\bar{g}_{11} + \frac{1+\sqrt{3}i}{2}\sigma_{02}\bar{g}_{02}\\
&\quad - \frac{3-3\sqrt{3}i}{4}\sigma_{11}\sigma_{20} - \frac{3-\sqrt{3}i}{2}|\sigma_{11}|^2,\\
\tilde{\sigma}_{12} &= \sigma_{02}g_{20} + \frac{3+\sqrt{3}i}{2}\sigma_{11}g_{11} + 2\bar{\sigma}_{11}g_{02} + \frac{1}{2}\bar{\sigma}_{20}g_{11} + g_{12}\\
&\quad - \frac{3+\sqrt{3}i}{2}\sigma_{11}^2 - \frac{3-\sqrt{3}i}{4}\sigma_{11}\bar{\sigma}_{20} + \frac{1-\sqrt{3}i}{2}\sigma_{11}\bar{g}_{20}\\
&\quad - \sqrt{3}i\sigma_{02}\bar{\sigma}_{11} + \frac{1+\sqrt{3}i}{2}\sigma_{02}\bar{g}_{11} + \frac{1-\sqrt{3}i}{2}\sigma_{20}g_{02},
\end{aligned}
$$

$$\tilde{\sigma}_{03} = \frac{1}{2}\sigma_{02}g_{11} + \bar{\sigma}_{20}g_{02} + g_{03} + \frac{1+\sqrt{3}i}{2}\sigma_{11}g_{02} + \frac{3-\sqrt{3}i}{4}\sigma_{02}\bar{\sigma}_{20} + \frac{1+\sqrt{3}i}{2}\sigma_{02}\bar{g}_{20}.$$

E. $\tilde{\sigma}_{ij}$ in Eq (4.26)

$$\begin{aligned}
\tilde{\sigma}_{20} &= \frac{1+i}{2}\sigma_{20} + g_{20},\ \tilde{\sigma}_{11} = (-1+i)\sigma_{11} + g_{11},\ \tilde{\sigma}_{02} = \frac{1+i}{2}\sigma_{02} + g_{02},\\
\tilde{\sigma}_{30} &= \frac{1-i}{2}{\sigma_{20}}^2 + (1-i)g_{20}\sigma_{20} - \frac{1+i}{2}\sigma_{11}\bar{\sigma}_{02} + \frac{1}{2}g_{11}\bar{\sigma}_{02} + i\sigma_{11}\bar{g}_{02} + g_{30},\\
\tilde{\sigma}_{21} &= \frac{1+3i}{2}\sigma_{20}\sigma_{11} + (2+i)g_{20}\sigma_{11} - i\bar{g}_{11}\sigma_{11} + \frac{1-2i}{2}g_{11}\sigma_{20} + \bar{\sigma}_{11}g_{11}\\
&\quad + \frac{1}{2}g_{02}\bar{\sigma}_{02} + i\bar{g}_{02}\sigma_{02} + \frac{1+i}{2}|\sigma_{02}|^2 - (1-i)|\sigma_{11}|^2 + g_{21},\\
\tilde{\sigma}_{12} &= -(1+i){\sigma_{11}}^2 - \frac{1+i}{2}\bar{\sigma}_{20}\sigma_{11} + (1+i)g_{11}\sigma_{11} - i\bar{g}_{20}\sigma_{11} + (1-i)\bar{\sigma}_{11}\sigma_{02}\\
&\quad + i\bar{g}_{11}\sigma_{02} + 2g_{20}\sigma_{02} + \frac{1-i}{2}\sigma_{20}\sigma_{02} - i\sigma_{20}g_{02} + 2\bar{\sigma}_{11}g_{02} + \frac{1}{2}\bar{\sigma}_{20}g_{11} + g_{12},\\
\tilde{\sigma}_{03} &= \frac{1+i}{2}\bar{\sigma}_{20}\sigma_{02} - \frac{(1-i)}{2}\sigma_{11}\sigma_{02} + i\bar{g}_{20}\sigma_{02} + \frac{1}{2}g_{11}\sigma_{02} + i\sigma_{11}g_{02} + \bar{\sigma}_{20}g_{02} + g_{03}.
\end{aligned}$$

AIMS Press